Covenant Journal of Physical & Life Sciences (CJPL) Vol. 7 No. 2, Dec. 2019
ISSN: ***p. 2354 – 3574 e. 2354 – 3485***

An Open Access Journal Available Online

Covenant Journal of Physical & Life Sciences

Vol. 7 No. 2, Dec. 2019

A Publication of Covenant University

Editor-in-Chief: Prof. Banke Ogunlana
banke.ogunlana@covenantuniversity.edu.ng

Managing Editor: Edwin O. Agbaike
edwin.agbaike@covenantuniversity.edu.ng

URL: ***http://journals.covenantuniversity.edu.ng/index.php/cjpls***

ISSN: ***p. 2354 – 3574 e. 2354 – 3485***

Published by Covenant University Journals,
Covenant University, Canaanland, Km 10, Idiroko Road,
P.M.B. 1023, Ota, Ogun State, Nigeria

Printed by Covenant University Press

URL: ***http://journals.covenantuniversity.edu.ng/index.php/cjpls***

Articles

Covenant Journal of Physical & Life Sciences (CJPL) Vol. 7 No. 2, Dec. 2019
ISSN: ***p. 2354 – 3574 e. 2354 – 3485*** **DOI:**

An Open Access Journal Available Online

Prevalence and Antibacterial Susceptibility of Selected Bacteria in the Urine of Biology Students at Tai Solarin University of Education

***Sebiomo Adewole & Ojo Folasade Tinuade**

Department Of Biological Sciences, Tai Solarin University of Education Ijagun, Ijebu-Ode
*rev20032002@yahoo.com;

Received: xxxx xxxxxx, 2019 Accepted: xxxx xxxxxx,, 2019
Date of Publication: December, 2019

Abstract**:** Urinary tract infection is a condition where one or more urinary structures become infected by the presence and growth of microorganisms that overcome the structures. This research work investigated the prevalence and antibacterial susceptibility of selected bacteria in the urine of biology students of Tai Solarin University of Education, Ijagun, Ogun State, Nigeria. Demographic survey of the students was determined. A 30 morse gauge, 3.26 mm calibrated wire loop capable of delivering 0.001 ml of urine was used for culturing on Blood Agar and MacConkey agar. The culture plates were incubated aerobically at 37˚C for 24 hours. Antibiotic susceptibility testing of the isolated test organisms was determined. Twenty-two percent of the respondents' used antibiotic in the past 14 days while 78% of the respondents did not use antibiotics in the past 14 days. All the twenty-five female students tested for the presence of *Escherichia coli*, *Staphylococcus aureus*, and *Klebsiella pneumoniae* in their urine tested positive to these pathogenic bacteria, although some in asymptomatic form. The highest *Escherichia coli*, *Staphylococcus aureus*, and *Klebsiella pneumoniae*, counts of $2.41\pm0.00 \times 10^5$ CFU/ml, $5.59\pm0.00 \times 10^5$ CFU/ml and $1.86\pm0.00\ 10^5$ CFU/ml

respectively were obtained in the urine samples of the female and male students. The highest Total Bacteria count of $4.77\pm0.00 \times 10^5$ CFU/ml was obtained in the female urine samples. Gentamicin showed highest zone of inhibition in *K. pneumonia* culture plateswith a mean value of 2.83 mm followed by erythromycin (2.51 mm) and ampicillin (2.48 mm).

Keywords: Susceptibility, Antibiotics, Inhibition, Urine, Bacteria

Introduction

The urinary tract is made up of organs (such as kidneys, ureters, bladder and urethra) that collects stores and releases urine from the body. Urinary tract infection is a condition where one or more urinary structures become infected by the presence and growth of microorganisms that overcome the structures. Urinary tract infections are one of the most common bacterial infections in the human urinary system including lower urinary tract such as bladder and urethra [1].

Diagnosis therefore cannot be made without bacteriological analysis of urine. Urinary tract infections (UTIs) such as cystitis and pyelonephritis are the most common infectious diseases in children. Bacteria causing urinary tract infection (UTI) is the most common found in developing countries like Nigeria where proper sanitization is not adequately considered. It has been reported that more than 150 million people are affected by UTI globally and it has also been estimated that about 30,000 UTI patients are treated in clinical wards [1].

Acute and uncomplicated UTI are most commonly found in women and it has been estimated that more than 60% women have UTI at least once in their lifetime. It has also been reported that the rate of causing UTI is 10.57% higher in sexually active females and teenage girls than males and the most common bacteria involved are *Escherichia coli* (32.8%), *Klebsiella pneumonia* (22.4%) and *Staphylococcus aureus* (15.1%). *E. coli* is the most common bacteria implicated in UTI infections. It causes 75-90% uncomplicated UTI [2].

Microbial invasion being the basis of urinary tract infection could be seen in various clinical manifestations resulting in various disease conditions in both males and females of all ages. Females are most at risk of bacteriuria. For example, in the United States, UTIs result in approximately 8 million physician visits and more than 100, 000 hospital admissions per year of sexually active women treated annually for UTIs. Up to 95% of the UTI cases in the U.S are treated with antibiotics such as cotrimoxazole without bacteriological investigation since these infections are routinely encountered in medical practice. This kind of indiscriminate use of antibiotics is however fraught with the problem of pathogen resistance to antibiotics [3]. Asymptomatic UTIs occur when urinary tract pathogens enter into the bladder without causing apparent symptoms. Typically, the pathogens are usually eliminated by host defense factors when they persist only for a short time in the human host. However, when such pathogens stay in the urinary system for a long time symptomatic urinary tract infection result [3].

Antimicrobial resistance among urinary tract isolates have recently been reported with an increased frequency all over the world. Several studies also have reported that the incidence of UTI has been increasing recently and its treatment has become more complicated because of the emergence of pathogens with increasing resistance to antimicrobial agents. It is necessary to identify the causative agent and spectrum of its antimicrobial susceptibilities in order to treat UTI. Since this spectrum may vary among geographical locations, hospitals and also in different age groups, each institution should carefully plan their antibiotic therapy.

Hence there is need to investigate the prevalence and antibacterial susceptibility of selected bacteria in the urine of biology students.

Materials and Methods

Collection of Samples

Mid-stream urine was collected from apparently healthy undergraduates of TASUED, (25 males and 25 females). The samples were collected into sterile plastic disposable bottles, refrigerated and examined within 2 - 4 hours of collection. The University student population was well known to be a high-risk segment of the community due to age, sex, and sexual activities among other predisposing factors. Students on antibiotic treatment within one week of the study were avoided.

Demographic Survey

A Demographic survey of all the students were determined to include age, sex, use of toilets, use of antibiotics and changes observed after antibiotics use. All these information were collected via the distribution of questionnaires to all the fifty students involved in this research.

Bacteriology

Samples were examined using standard methods as adopted by Ayoade [3]. A 30 Morse gauge, 3.26 mm calibrated wire loop capable of delivering 0.001 ml of urine was used for culturing on Blood Agar and MacConkey agar. The culture plates were incubated aerobically at 37˚C for 24 hours. Culture plates without visible growth were further incubated for an additional 24 hours before being discarded. The number and types of colonies grown on the medium were recorded as being insignificant when samples gave a colony count of less than 10^4 CFU/ml. Samples with colony count equal to or greater than approximately 10^5 CFU/ml of the urine samples was considered to have significant bacteriuria. Bacterial isolates were identified based on a combination of cultural, morphological and biochemical characteristics.

Antimicrobial Susceptibility Testing

Antibiotic susceptibility testing of the isolated test organisms, was carried out using the following antibiotics: Penicillin, Chloramphenicol, Ampicillin, Gentamycin and Erythromycin,. The nutrient broth was prepared according to the manufacturer's specification and 10 ml was dispensed into sterile test tubes. A sterile loop was used to pick a pure colony of the test isolate and emulsified in the nutrient broth. The nutrient agar was then incubated at 37˚C for 18 - 24 hours. Normal saline was prepared using sodium chloride and distilled water and the normal saline was

sterilized using the autoclave for 15 minutes at 121˚C then allowed to cool. Then the test organism was placed in 10 ml of the normal saline in a test tube then incubated for 2 hours. Turbidity standard of 0.5 Mc Farland was used, this is barium sulphate standard against which the turbidity of the test and control inocula was compared, when matched with the standard the inocula gives almost confluent growth.

A sterile swab was used to inoculate the Mueller Hinton agar previously prepared by putting the sterile swab into the inocula and rotating the swab against the side of the test tube above the level of the suspension. The swab was used to streak the surface of the Mueller Hinton Agar plates in three directions, rotating the plates in approximately 60˚C to ensure even distribution with a sterile forceps. The approximate antimicrobial sterile discs were placed evenly distributed on the inoculated plates. The plates were inverted and incubated aerobically at 37˚C and examined after 18 - 24 hours incubation and from the underside of the plates. A ruler was used to measure the diameter of the zone of inhibition in millimetres. The reaction of the test organism to each antibiotic was reported as sensitive, intermediate or resistant on the basis of zone of inhibition.

Data Analysis

The data were statistically analysed, with SPSS version 20 software, using a one-way analysis of variance (ANOVA)

Results

Table 1 shows the age and sex distribution of students used for the study. The table shows that 25 males and 25 females partook in the study. The table also shows that age group of 15-19 (25) partook of the study than other age group

Table 1: A Summary of the Age and sex distribution of students used for the study

Age distribution	No of Males examined	No. of Females examined	Frequency of individual by Age-group
15-19	12	13	25
20-24	9	10	19
25 and above	4	2	6

Table 2 shows the type of toilet used by the respondents. The table showed that 84% of the respondents use water closet while 16% of the respondents use pit latrine. The result shows that majority of the respondents use water closet.

Table 2: Summary of the toilet used by the respondents

Type of toilet	Frequency	Percentage
Pit Latrine	8	16%
Water Closet	42	84%

Table 3 shows that 22% of the respondents' used antibiotic in the past 14 days while 78% of the respondents did not use antibiotics in the past 14 days.

Table 3: Summary of antibiotics in the past 14 days.

Antibiotic for the past 14 days	Frequency	Percentage
Yes	11	22%
No	39	78%

Table 4 shows the summary of changes after taking antibiotics. The table shows that 100% of the respondents were of the view that there are changes after taking the antibiotics.

Table 4: Summary of changes after taking antibiotics

Changes after taking Antibiotics	Frequency	Percentage
Yes	10	100%
No	-	0%

Table 5, shows the total count of *Escherichia coli*, *Staphylococcus aureus*, and *Klebsiella pneumoniae* obtained from the urine samples of all the female students tested. All the twenty-five female students tested for the presence of *Escherichia coli*, *Staphylococcus aureus*, and *Klebsiella pneumoniae*in their urine tested positive to these pathogenic bacteria, although some in asymptomatic form, showing the carrier status of these female students. These shows that the organisms tested were 100% prevalent in all the female urine samples tested. Similarly, in Table 6, all the twenty-five male students tested showed 100% prevalence of *Escherichia coli*, *Staphylococcus aureus*, and *Klebsiella pneumoniae*in their urine samples. The highest *Escherichia coli*, *Staphylococcus aureus*, and *Klebsiella pneumoniae*, counts of $2.41\pm0.00 \times 10^5$ CFU/ml,$5.59\pm0.00 \times 10^5$ CFU/ml and $1.86\pm0.00\ 10^5$ CFU/ml respectively were obtained in the urine samples of the female and male students. The highest Total Bacteria count of $4.77\pm0.00 \times 10^5$ CFU/ml was obtained in the female urine samples (Table, 5), while the highest Total Bacteria Count of$4.13\pm0.00 \times 10^5$ CFU/ml was obtained in the male urine samples (Table 6).

Table 5: The Total Bacterial, *E. coli*, *S. aureus* and *K. pnneumoniae* counts ($\times 10^5$ CFU/ml) in female urine samples

S/N	Sample	Total count	*E.coli*	*Staphylococcus auerues*	*K.pneumoniae*
1	F_{11}	3.83 ± 0.00^a	1.75 ± 0.10^b	2.95 ± 0.10^b	$1.16\pm.000^a$
2	F_{26}	3.90 ± 0.00^a	1.77 ± 0.10^b	3.54 ± 0.10^b	1.30 ± 0.00^a
3	F_{22}	3.93 ± 0.00^a	$1.93\pm.0.10^b$	3.69 ± 0.10^b	1.33 ± 0.17^c
4	F_{40}	4.10 ± 0.00^a	1.95 ± 0.10^b	4.40 ± 0.81^c	134 ± 0.90^d
5	F_{35}	4.19 ± 0.77^d	1.96 ± 0.10^b	4.64 ± 0.00^a	1.36 ± 0.12^c
6	F_5	4.30 ± 0.67^c	1.97 ± 0.10^a	4.06 ± 0.10^a	1.39 ± 0.15^b
7	F_{20}	4.31 ± 0.00^a	1.97 ± 0.10^b	4.50 ± 0.10^b	1.41 ± 0.47^c
8	F_{49}	4.32±0.00a	1.80 ± 0.10^b	4.07 ± 0.10^b	1.46 ± 0.10^b
9	F_{19}	4.35 ± 0.00^a	2.10 ± 0.10^b	4.07 ± 0.00^a	1.49 ± 0.10^b
10	F_{28}	4.39 ± 0.11^c	2.12 ± 0.10^b	4.08 ± 0.00^a	1.53 ± 0.15^d
11	F_{14}	4.40 ± 0.11^c	2.18 ± 0.10^b	4.03 ± 0.10^b	1.59 ± 0.00^a
12	F_{16}	4.41 ± 0.97^d	2.20 ± 0.10^b	4.08 ± 0.00^a	1.62 ± 0.20^c
13	F_{13}	$4.46\ \pm0.63^c$	2.22 ± 0.10^b	4.12 ± 0.00^a	1.64 ± 0.73^d
14	F_9	4.50 ± 0.14^b	2.22 ± 0.19^c	4.14 ± 0.10^a	1.73 ± 0.51^d
15	F_{50}	4.02 ± 0.57^c	2.22 ± 0.19^b	4.27 ± 0.00^a	1.75 ± 0.00^a
16	F_6	4.55 ± 0.00^a	$2.24\pm.010^b$	4.69 ± 0.00^a	1.76 ± 0.00^a

17	F_{30}	4.59±0.00[a]	2.25±0.10[c]	4.75±0.10[c]	1.80±0.01[b]
18	F_4	4.60±0.01[a]	2.25±0.30[b]	4.83±0.01[a]	1.81±0.51[c]
19	F_{34}	4.62±0.00[a]	2.25±0.10[b]	4.94±0.00[a]	1.82±0.00[a]
20	F_{29}	4.66±0.21[d]	2.26±0.01[b]	5.07±0.15[c]	1.83±0.00[a]
21	F_{27}	4.70±0.00[a]	2.28±0.00[a]	5.22±0.47[c]	1.84±0.01[b]
22	F_3	4.70±0.00[a]	2.37±0.01[b]	5.46±0.11[c]	1.84±0.51[d]
23	F_{12}	4.74±0.00[a]	2.38±.0.00[a]	5.47±0.11[b]	1.85±0.00[a]
24	F_{15}	4.77±0.00[a]	2.40±0.00[a]	5.48±0.10[b]	1.86±0.00[a]
25	F_{10}	4.77±0.00[a]	2.41±0.00[a]	5.59±0.00[a]	1.80±0.01[b]

Mean with the same superscripts in the same column or row are not significantly different but mean with different superscripts are significantly different using DMRT at (P<0.05)

Table 6: The Total Bacterial, *E. coli*, *S. aureus* and *K. pnneumoniae* counts ($\times 10^5$ CFU/ml) in male urine samples

S/N	Sample	Total count	*E.coli*	*Staphylococcus aureus*	*K.pneumonia*
1	M_8	3.20±0.00[a]	1.22±0.10[b]	2.85±0.10[b]	1.19±.000[a]
2	M_{13}	3.30±0.00[a]	1.41±0.10[b]	2.90±0.10[b]	1.23±0.00[a]
3	M_9	3.50±0.00[a]	1.48±.0.10[b]	3.19±0.10[b]	1.33±0.17[c]
4	M_{15}	3.50±0.00[a]	1.60±0.10[b]	3.26±0.81[c]	134±0.90[d]
5	M_7	3.56±0.77[d]	1.65±0.10[b]	3.30±0.00[a]	1.36±0.12[c]
6	M_6	3.61±0.67[c]	1.70±0.10[a]	3.33±0.10[a]	1.39±0.15[b]
7	M_1	3.64±0.00[a]	1.73±0.10[b]	3.50±0.10[b]	1.41±0.47[c]
8	M_{20}	3.70±0.00[a]	1.80±0.10[b]	3.70±0.10[b]	1.46±0.10[b]
9	M_5	3.37±0.00[a]	1.82±0.10[b]	3.77±0.00[a]	1.49±0.10[b]
10	M_{21}	3.77±0.11[c]	1.83±0.10[b]	3.81±0.00[a]	1.53±0.15[d]
11	M_{22}	3.81±0.11[c]	1.85±0.10[b]	3.93±0.10[b]	1.59±0.00[a]
12	M_{18}	3.86±0.97[d]	1.90±0.10[b]	4.08±0.00[a]	1.62±0.20[c]
13	M_{25}	3.97 ±0.63[c]	1.97±0.10[b]	4.12±0.00[a]	1.64±0.73[d]
14	M_{14}	3.99±0.14[b]	2.00±0.19[c]	4.14±0.10[a]	1.73±0.51[d]
15	M_{24}	4.02±0.57[c]	2.06±0.19[b]	4.27±0.00[a]	1.75±0.00[a]
16	M_{23}	4.02±0.00[a]	2.10±.010[b]	4.69±0.00[a]	1.76±0.00[a]
17	M_{10}	4.11±0.00[a]	2.12±0.10[c]	4.75±0.10[c]	1.80±0.01[b]
18	M_2	4.10±0.01[a]	2.15±0.30	4.83±0.01[a]	1.81±0.51[b]
19	M_{11}	4.12±0.00[a]	2.22±0.10[b]	4.94±0.00[a]	1.82±0.00[a]
20	M_3	4.11±0.21[d]	2.36±0.10[b]	5.07±0.15[c]	1.83±0.00[a]
21	M_{17}	4.12±0.00[a]	2.37±0.00[a]	5.22±0.47[b]	1.84±0.01[a]
22	M_{16}	4.13±0.00[a]	2.37±0.01[b]	5.46±0.11[c]	1.84±0.51[d]
23	M_{12}	4.12±0.00[a]	2.38±.0.00[a]	5.47±0.11[b]	1.85±0.00[a]
24	M_{19}	4.10±0.00[a]	2.40±0.00[a]	5.48±0.10[b]	1.86±0.00[a]
25	M_4	4.13±0.00[a]	2.41±0.00[a]	5.59±0.00a	1.80±0.01[d]

Mean with the same superscripts in the same column or row are not significantly different but mean with different superscripts are significantly different using DMRT at (P<0.05)

Table 7 shows the zones of inhibition of three bacteria. Gentamicin showed highest zone of inhibition in *K. pneumonia* culture plates with a mean value of 2.83 mm followed by erythromycin (2.51 mm) and ampicillin (2.48 mm). Penicillin showed the lowest zone of inhibition with a mean value of 1.55 mm. Also, Erythromycin showed

the highest zone of inhibition in *Esherichia coli* culture plates with a mean value of 3.60 mm followed by Gentamicin (3.30 mm) and ampicillin (3.16 mm). Chloramphenicol shows the lowest zone of inhibition with a mean value of 2.20 mm. Also, Erythromycin shows highest zone of inhibition in the treatment of *Staphylococcus aureus* with a mean value of 5.67 mm followed by Gentamicin with a mean value of 5.58 mm, followed by Chloramphenicol with a mean value of 4.40 mm. Ampicillin showed the lowest zone of inhibition with a mean value of 4.20 mm.

Table 7: The zones of inhibition (mm) of various antibiotics of three bacteria

Bacteria	Penicillin	Chloramphenicol	Ampicillin	Gentamicin	Erythromycin
K. pneumonia	1.55^a	1.80^a	2.48^a	2.83^a	2.51^a
Esherichia coli	2.77^b	2.20^b	3.16^b	3.30^b	3.60^b
Staphylococcus aureus	4.50^c	4.40^c	4.20^c	5.58^c	5.67^c

Discussion

Urinary tract infection caused by microorganisms is one of the most common infections in the world. Increasing resistance to broad spectrum antibiotics of urine pathogens especially *E. coli* and *K. pneumonia* as the prevalent UTIs pathogens is alarming. The rapid and correct choice of the antibiotic enables rapid cure of the patient, and sometimes even to save the patient's life. So, it is very important to determine the antibiotic resistance patterns of UTIs pathogens. It was discovered in this study that the infection subsided after the use of antibiotics. Widespread inappropriate use of antimicrobial agents in Nigeria is also due to the possibility of buying antibiotics from pharmacy stores with or without prescription; this is a significant contributing factor to the development of resistance to antimicrobial agent

Five antibiotics, Penicillin, Chloramphenicol, Ampicillin, Gentamycin and Erythromycin were found to be all effective for all the Gram-negative organisms isolated in this study particularly *E. coli* and *Staphylococcus aureus* while Gentamycin was found to be effective for the gram-positive organisms. Abejew [1] reported that Pseudomonas and Proteus species were resistant to almost all antibiotics except Gentamycin.

The result of the study indicates that *E. coli, S. aureus*and *K. pneumoniae* are among the most common types of bacteria found in the urine sample of undergraduates causing UTIs. This result agrees with other reports that indicate that *E. coli* is the commonest pathogen isolated in patients with UTI [4,5]. *Staphylococcus aureus* was observed to be sensitive to almost all the antibiotics tested, though to varying degrees. The results in this study which showed that *E. coli* wassusceptible toerythromycin, Gentamycin, ampicillin, chloramphenicol and penicillin, at inhibition zone values of 3.60 mm 3.30 mm, 3.16 mm, 2.20 mm and 2.77 mm respectively, were found to be similar to the observations of Nwanze *et al*.[6]. Ako-Nai *et al*.[7] presented a report in which 67.3% of *E.coli* isolates were resistant to

ampicillin, 64.9% resistant to amoxicillin, 51.8% to penicillin, 70.2% to tetracycline, 48.8% to erythromycin, 36.9% to Gentamycin, 11.9% to chloramphenicol and 1.8% to gentamycin in a study Ibadan, Nigeria. S. *faecalis* had a profile of 70.7% (ofloxacin), 70.4% (augmentin), 60.3% (erythromycin)and a susceptibility of equal to or higher than 50.0% to chloramphenicol, pefloxacin, nitrofurantoin, colistin and streptomycin, while a susceptibility of less than 50.0 % to gentamycin, nalidixic acid, tetracycline and cotrimoxazole similar to the data presented by Nwanze *et al.*[6].

Recommendations

- Regular monitoring is required to establish reliable information about resistance pattern of urinary pathogens for optimal empirical therapy of patients with UTIs.
- Empirical antibiotic selection should be based on the knowledge of local prevalence of bacterial organisms and antibiotic sensitivities rather than on universal guidelines.
- Periodic epidemiological studies such as the one being reported here will also help in identifying the important UTI pathogens with a view to developing an effective and proper treatment model. Moreover, infection from UTI-causing pathogens can be drastically reduced when intermediate hosts of UTI-causing parasites are eradicated and by improved personal hygiene.
- Furthermore, public health education should be given to the public concerning the prudent use of antibiotics so as to avoid the problem of antibiotic resistance. Additionally, legislation is required to enforce proper use of animal and human medicines to minimize cross-transmission of resistant genes from animals to humans and vice versa.
- There is need to monitor the profile of etiological bacteria of UTIs and the antimicrobial resistance regularly. This would show emergence of resistance to newer therapeutic agents as well as keep track of effectiveness of serving therapeutic agents.
- Health workers should mobilize patients to ensure that they have duly completed the prescribed antimicrobial therapy as not finishing it leads to resistance.
- Parents should not assume their children automatically need antibiotics and should not routinely ask for them when their children are sick this will greatly reduce antimicrobial resistance instead they should seek a physician's advice.

Conclusion

The study has shown an overview of the most common pathogenic bacteria found among undergraduates compared to other studies. *Escherichia coli* and *Klebsiella pneumoniae* were the most predominant strains in urine tract infection (UTI).

Suggestion for further studies

Several future research gaps worth filling is recommended. There is need to

establish the influence of resistance of recurrent UTIs, and the risk factors involved in infection with resistant bacteria strain. Elaboration of the in vivo effectiveness of the commonly used antimicrobial agents and investigation of the endogenous nature of the identified uropathogenic isolates are other fruitful future research areas.

References

[1]Abejew, A.A., Denboba, A.A. and Mekonnen, A.G. (2014) Prevalence and antibiotic resistance pattern of urinary tract bacterial infections in Dessie area, North-East Ethiopia. BMC Res. Notes, 7: 1-7.

[2] Ejrnaes, M., Arsalane, L., El Kamouni, Y. and Zouhair, S. (2012) Antimicrobial Susceptibility of Urinary K. pneumonia and the Emergence of Carbapenem-Resistance Strain. Afr. J. Urology, 21: 36-40.

[3] Ayoade, F., Moro, D. D. and Ebene, O. L. (2013) Prevalence and Antimicrobial Susceptibility Pattern of Asymptomatic Urinary Tract Infections of Bacterial and Parasitic Origins among University Students in Redemption Camp, Ogun State, Nigeria. Open J. Med. Microbiol., 3: 219-226

[4] Akinyemi, K.O., Alabi, S.A., Taiwo, M.A. and Omonigbehin, E.A. (1997). Antimicrobial susceptibility pattern and plasmid profiles of pathogenic Bacteria isolated from subjects with urinary tract infections in Lagos,Nigeria. Nig. Quarterly J. Hosp. Med., 1: 7-11

[5] Ebie, M.Y., Kandakai-Olukemi, Y.T., Ayanbadejo J. and Tanyigna, K.B. (2001). Urinary Tract Infections in a Nigerian Military Hospital. Nig. J. Microbiol., 15 (1): 31-37

[6] Nwanze, P. I., Nwaru, L. M., Oranusi, S.1, Dimkpa, U., Okwu, M. U., Babatunde, B. B., Anake, T. A., Jatto, W. and Asagwara, C. E. (2007).Urinary tract infection in Okada village: Prevalence andantimicrobial susceptibility pattern. Sci. Res. and Essays, 2(4): 112-116

[7] Ako-Nai, A.K., Adeyemi, F.M., Aboderin, O.A. and Kassim, O.O. (2005). Antibiotic resistance profile of Staphylococci from clinical sources recovered from patients. Afr. J. Biotechnol., 4(8): 816-822

Covenant Journal of Physical & Life Sciences (CJPL) Vol. 7 No. 2, Dec. 2019
ISSN: ***p. 2354 – 3574 e. 2354 – 3485*** **DOI:**

An Open Access Journal Available Online

The Utilization of Glyphosate by Bacteria Isolated from Soil

Faith Onyinyechi Mbagwu, Oluwafemi Adebayo Oyewole, Solomon Bankole Oyeleke & *Olabisi Peter Abioye

Department of Microbiology
Federal University of Technology, PMB 65, Minna, Nigeria
bisyem2603@gmail.com

Received: xxxx xxxxxx, 2019 Accepted: xxxx xxxxxx,, 2019
Date of Publication: December, 2019

Abstract: Glyphosate is one of the most commonly used herbicides worldwide. It is primarily applied to agricultural lands. This study examined the utilization of glyphosate by bacteria isolated from soil. Five bacteria were isolated, namely; Bacillus cereus, Bacillus subtilis, Escherichia coli, Pseudomonas sp., and Actinomyces sp. Bacillus cereus and Bacillus subtilis were selected for the studies based on their rapid degradation of the herbicides. The ability of the isolates to degrade different concentrations of glyphosate were tested in minimal salt medium (MSM) and incubated on a rotary shaker at 120 rpm at 30ºC for 28 days. The effects of Pb^{2+} and Cd^{2+} on degradation of the isolates were also determined at concentrations of 200 µg/ml, 300 µg/ml and 400 µg/ml in 150 ml of the MSM. The bacteria were isolated using pour plate method and identified based on their cultural and biochemical characteristics. The two isolates were identified as Bacillus cereus BFM4 and Bacillus subtilis H184 using polymerase chain reaction and sequence analysis. There were significant differences ($P < 0.05$) in the percentage utilization of the herbicides by the test organisms in all the treatments at day 28. Bacillus cereus BFM4 had the highest percentage utilization of 97.04 % and 90.49 % of glyphosate at the lowest concentration 20 mg/ml and 400 µg/ml of Pb^{2+}. The results of this study showed that the isolates were able to utilize varying concentration of glyphosate with an increased utilization on addition of Pb^{2+} and Cd^{2+}.

Keywords: Utilization, Bacillus cereus, Bacillus subtilis, glyphosate, heavy metals.

URL: ***http://journals.covenantuniversity.edu.ng/index.php/cjpls***

Introduction

Herbicides are used extensively in agriculture for the control of many annual and perennial weeds [1]. However, the indiscriminate use of herbicides may result in weed resistance or alter the biological functions of soil; additionally, herbicides can have extensive unintended effects on nutrient availability and disease severity [2] resulting from direct herbicide-induced weakening of plant defenses and increased pathogen population and virulence

Herbicides applied to the environment have shown to have long term residual effects while others have shown to have acute fatal effects when not properly handled. Organochlorine herbicides for example have shown to be persistent in the environment, the result of which find their way to contaminate ground water, surface water, food products, air, soil [3]. Herbicides can enter the human body through inhalation of aerosols, dust and vapor that contain herbicides; through oral exposure by consuming contaminated food and water; and through dermal exposure by direct contact of pesticides with skin [1].

The effects of herbicides on human health are harmful based on the toxicity of the chemical and the length and magnitude of exposure [4]. Farm workers and their families experience the greatest exposure to agricultural pesticides through direct contact with the chemicals. Children are most susceptible and sensitive to herbicides due to their small size and underdevelopment. The chemicals can bioaccumulate in the body over time. Exposure to pesticides can range from mild skin irritation to birth defects, tumors, genetic changes, blood and nerve disorders, respiratory diseases, reproduction disorders, endocrine disruption, and even coma or death [5]. It is this aspect of herbicide in the environment that has raised concern among environmental scientists to study their behaviour in the environment and then come out with a sound alternative so as to rescue the human population from their adverse effects.

Herbicide may eliminate plants and animals essential to the functioning of the entire, promote the dominance of undesired species, or may simply decrease the number and variety of species present in the community. This may disrupt the dynamics of the food webs in the community by breaking the existing dietary linkages between species. This has created a further dependence on herbicides. The effects of herbicides on the biodiversity of plants and animals in agricultural landscapes, whether caused directly or indirectly by herbicides, constitute a major adverse environmental impact of herbicides [1].

Glyphosate (N-(phosphonomethyl) glycine), which is commonly called Roundup is one of the most commonly used herbicides worldwide [6]. It is primarily applied to agricultural lands. Glyphosate is also popular in production forestry because of its effectiveness in controlling many understory plant species, benign effects on conifers, low mammalian toxicity, and rapid inactivation in soil [1]. It is a phosphorus containing amino acid that functions both as a sole phosphorus source for in vitro microbial growth and as a readily available carbon and nitrogen source when degraded in soil.

The potential non-target effects of glyphosate on soil microorganisms and their processes, such as nutrient cycling and maintenance of soil structure, are of concern. Glyphosate inhibits protein synthesis via the shikimic acid pathway

in bacteria and fungi and one of its surfactants, polyoxyethylene tallow amine, is toxic to species of bacteria and protozoa [7].Because of the impact of herbicides on soil microbial ecosystems and agriculture, it is important to identify methods for enhancing herbicide degradation. Several treatment processes are available for removing herbicides, including biodegradation, filtration, adsorption, membrane technique, chemical, hydrolytic, and photolytic degradation [8].

Biodegradation of herbicides by microbial agents such as bacteria is an eco-friendly, cost effective, highly efficient approach and can be considered as a superior alternative to physical and chemical methods which are not only technically laborious and costly; also are not sufficient to completely degrade organic toxins present in herbicides. Microorganisms have a lot of metabolic diversity which makes it easy for them to metabolize herbicides. Microorganisms has the capacity to completely mineralize herbicides into simpler compounds such as carbon dioxide (CO_2) and water (H_2O) which are considered as non-harmful byproducts. Biodegradation of herbicides is important in terms of sustainability, because the microbial agents that are involved in carrying out the biodegradation process are always in the environment and so one does not need to buy them from the market [8, 9]. The use of bacteria (e.g. species of Pseudomonas, Bacillus) for degradation and detoxification of numerous toxic chemicals such as herbicides is an effective tool to decontaminate the polluted agricultural sites. Isolation of indigenous bacteria and yeasts capable of metabolizing herbicides provides environmentally friendly means of in situ detoxification. Many herbicide-degrading genes in soil bacteria have been reported to be encoded on plasmids [5]. The aim of this research therefore was to study the growth of some soil microorganisms in glyphosate enriched minimal salt medium.

Materials and Methods

Collection of Samples

A soil sample was collected with a sterile soil auger from a depth of 0-15 cm from four different sites within Federal University of Technology Botanical Garden, Bosso campus, Minna. Soil samples from each site was thoroughly mixed and placed in sterile polyethylene bags. This was transported immediately to Microbiology laboratory of the University and stored at 4^oC before use within 72 hours [10]. Glyphosate 41% SL was purchased from Brains and Strength Company limited, Maikunkele, Minna, Nigeria. The choice for this herbicide was because it is commonly used for the control of annual and biennial weeds in the study area.

Preparation of Isolation Medium

A Mineral Salts Medium (MSM)consisting of $MgSO_4.7\ H_2O$, 0.2g; K_2HPO_4, 1.8g; $FeSO_4.7H_2O$, 0.01 g;NH_4Cl, 4.0 g; NaCl, 0.1 g; KH_2PO_4, 1.2 g in 1000 ml of distilled water was used. All glass wares were washed with 1M HCl and thoroughly rinsed with deionized water to remove contaminating phosphate before use. The medium was autoclaved at 121^oC for 15 minutes [11].

Isolation of Herbicides Utilizing Bacteria

Herbicide utilizing bacteria were isolated by air-drying soil samples and sieving it using a 2 mm mesh. A soil sample (5 g) was suspended in 250 ml Erlenmeyer flask containing a mixture of 50 ml of mineral salts medium and 1 ml of the herbicide. The flask was incubated on a rotary shaker at 120 rpm for 24 hours at 30^{o}C. Isolation of bacteria was done using the pour plate method. The plates were incubated at 37^{0}C for 24 hours. Morphologically distinct colonies were isolated and repeatedly sub-cultured on nutrient agar. Identity of the isolates was affirmed after characterization by standard bacteriological methods and molecular technique.

Identification and Characterization of Bacterial Isolates

The isolates from the screening procedure were identified using microbiological and biochemical procedures such as Gram staining, spore staining, motility and citrate utilization tests [12].

Molecular Characterization of Bacteria Isolate

The molecular method employed included DNA extraction, amplification of copies of DNA using polymerase chain reaction using 16S rRNA gene. The 16S rRNA gene sequences were used in BLAST searches to determine the best similarity to sequences in the NCBI database (http://blast.ncbi.nlm.nih.gov/Blast.cgi).

Screening of Isolates for Herbicides Utilization

The isolates for herbicide utilization were screened by inoculating 1.0 ml portion of each isolate into 150-ml of mineral salt medium (contained in a 250-ml flask). It contained different concentrations of the herbicide (20, 30, 40 mg/ml of the herbicide). The flasks were incubated on a rotary shaker at 120 rpm for 180 h at 30^{o}C [13]. The ability of each isolate to utilize the herbicide was determined by spectrophotometry (Shimadzu UV, Model: UV-180, Japan) at 482 nm.

Effects of Different Concentrations of Heavy Metals on the Bacterial Isolates

Salts of the selected heavy metals ions Pb^{2+} and Cd^{2+}, at a concentration of 200 µg/ml, 300 µg/ml and 400 µg/ml were added to 150 ml of the mineral salts medium. The medium was autoclaved prior to the addition of different concentrations (20, 30, 40 mg/ml) of the filter-sterilized herbicides (size of the filter is 0.045 mm in diameter). Aliquot (1 ml) of each isolate was inoculated into the media and incubated at 30^{0}C for 28 days. Medium without heavy metals was used as control. Inoculated flasks were incubated at 30^{0}C on a rotary shaker at 120 rpm. Growth was assayed by measuring the optical density with a spectrophotometer (Shimadzu UV, Model: UV-180, Japan) at 482 nm [4].

Statistical Analysis

Statistical analysis of the data generated was carried out to indicate mean significant differences between the treatments using Statistical Package for Social Sciences (SPSS) version 16.0. One way analysis of variance (ANOVA) was used. Graphs and tables were used for data presentation.

Results

Bacterial Isolates Screened for Glyphosate Utilization

Five bacterial isolates were screened for glyphosate utilization by measuring their growth at 482 nm on medium containing glyphosate as sole carbon and phosphorous source. Of the five identified bacterial species, two (Bacillus subtilis and Bacillus cereus) were selected for further biodegradation studies based on their rapid utilization of glyphosate (Figure 1).

Molecular characteristics of bacterial isolates

The molecular characteristics of the bacterial isolates with the best ability to degrade the herbicide was determined as observed in Figure 2 showing the integrity of the amplified genes on agarose gel. The gel documented images of the isolated bacterial DNA after electrophoresis appeared at 1500 kb which indicated pure isolates. Lane Mk represents molecular marker (ladder). The result of the sequence analysis confirmed the isolates as Bacillus cereus strain BFM4 and Bacillus subtilis strain H184 using sequence analysis.

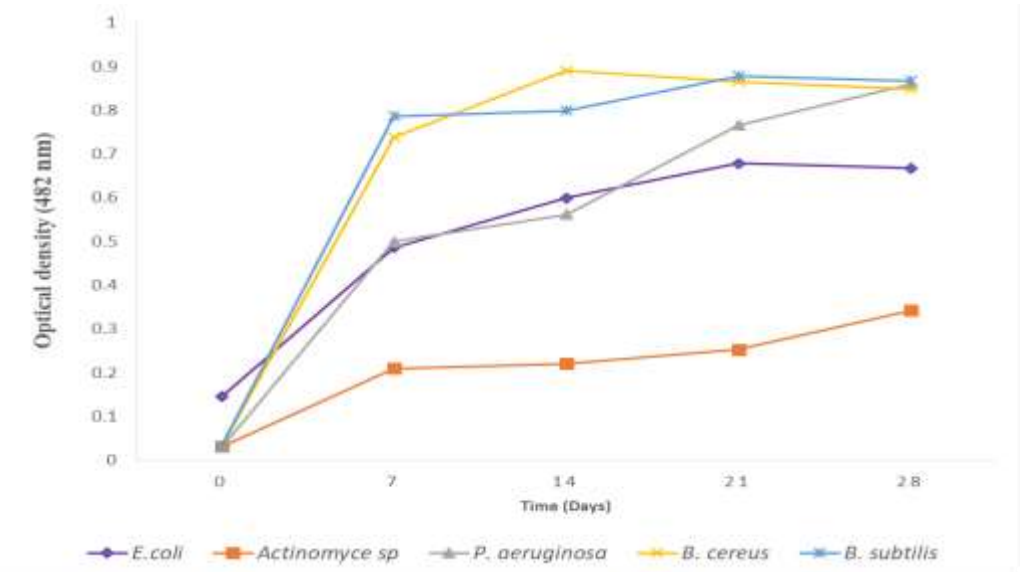

Figure 1: Bacterial isolates screened for glyphosate utilization

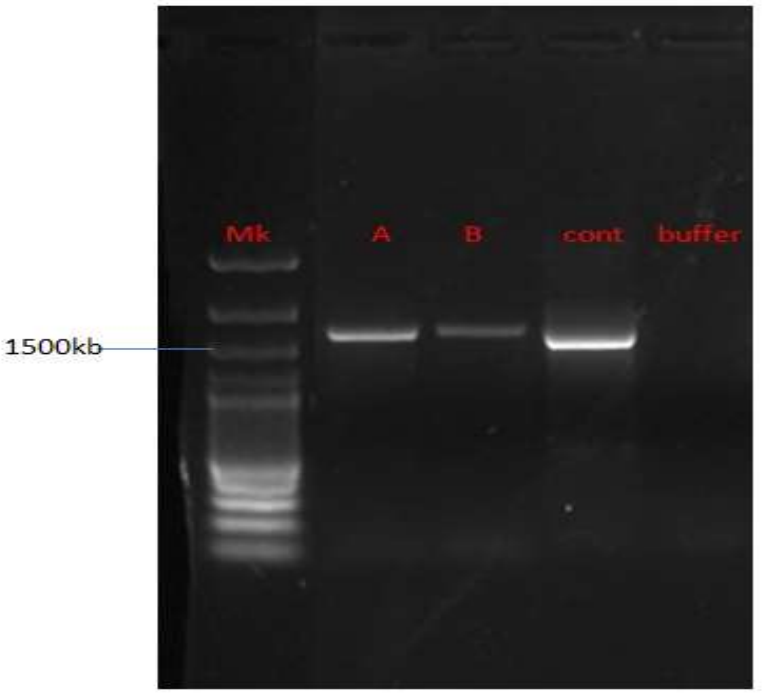

Figure 2: Capture gel electrophoresis showing size of the amplified genes
Keys:
A= *Bacillus cereus* strain BFM4, B= *Bacillus subtilis* strain H184, Control= *Lactobacillus plantarum*, Buffer= tris base, acetic acid, EDTA

Nucleotide sequence ofBacillus cereus strain BFM4 is as follows:

GGGCGCACTATACATGCAAGTCG
AGGGGACAGATGGGAGCTTGCTT
CCTGATGTTAGCGGCGGACGGGT
GAGTAACACGTGGGTAACCTGCC
TGTAAGACTGGGATAACTCCGGG
AAACCGGGGCTAATACCGGATGC
TTGTTTGAACCGCATGGTTCAAAC
ATAAAAGGTGGCTTCGGCTACCA
CTTACAGATGGACCCGCGGCGCA
TTAGCTAGTTGGTGAGGTAATGG
CTCACCAAGGCAACGATGCGTAG
CCGACCTGAGAGGGTGATCGGCC
ACACTGGGACTGAGACACGGCCC
AGACTCCTACGGGAGGCAGCAGT
AGGGAATCTTCCGCAATGGACGA
AGTCTGACGGAGCAACGCCGCGT
GAGTGATGAAGGTTTTCGGATCG
TAAAGCTCTGTTGTTAGGGAAGA
ACAAGTACCGTTCGAATAGGGCG
GTACCTTGACGGTACCTAACCAG
AAAGCCACGGCTAACTACGTGCC
AGCAGCCGCGGTAATACGTAGGT
GGCAAGCGTTGTCCGGAATTATT
GGGCGTAAAGGGCTCGCAGGCGG
TTTTTAAGTCTGATGTGAAAGCCC
CCGGCTCAACCGGGGAGGGTCAT
TGGAAACTGGGGAACTTGAGTGC
AGAAGAGGAGAGTGGAATTCCAC
GTGTAGCGGTGAAATGCGTAGAG
ATGTGGAGGAACACCAGTGGCGA
AGGCGACTCTCTGGTCTGTAACTG
ACGCTGAGGAGCGAAAGCGTGGG

GAGCGAACAGGATTAGATACCCT
GGTAGTCCACGCCGTAAACGATG
AGTGCTAAGTGTTAGGGGGTTTCC
GCCCCTTAGTGCTGCAGCTAACGC
ATTAAGCACTCCGCCTGGGGAGT
ACGGTCGCAAGACTGAAACTCAA
AGGAATTGACGGGGGCCCGCACA
AGCGGTGGAGCATGTGGTTTAAT
TCGAAGCAACGCGAAGAACCTTA
CCAGGTCTGACATCCTCTGACAAT
CCTAGAGATAGGACGTCCCCTTC
GGGGGCAGAGTGACAGGTGGTGC
ATGGTTGTCGTCAGCTCGTGTCGT
GAGATGTTGGGTTAAGTCCCGCA
ACGAGCGCAACCCTTGATCTTAGT
TGCCAGCATTCAGTTGGCACTCTA
AGGTGACTGCCGGTGACAAACCG
GAGGAAGGTGGGGATGACGTCAA
ATCATCATGCCCCTTATGACCTGG
GCTACACACGTGCTACAATGGAC
AGAACAAAGGGCAGCGAAACCG
GAGGTTAAGCCAATCCCACAAAT
CTGTTCTCAGTTCGGATCGCAGTC
TGCAACTCGACTGCGTGAAGCTG
GAATCGCTAGTAATCGCGGATCA
GCATGCCGCGGTGAATACGTTCC
CGGGCCTTGTACCCAACCGCCCGT
CACACCACGAGAGTTTGTAACAC
CCGAAGTCGGTGAGGTAACCTTTT
AGGAGCCAGCGGCCGAAGGTGGC
CAGA

Nucleotide sequence of Bacillus subtilis strain H184 is as follows:

GGAACGCGGGCGGCGTGCCTAAT
ACATCCAAGTCGAGCGAATAGAT
TAAGAGCTTGCTCTTATGAAGTTA
GCGGCGGACGGGTGAGTAACACG
TGGGTAACCTGCCCATAAGACTG
GGATAACTCCGGGAAACCGGGGC
TAATACCGGATAACATTTTGAACC
GCATGGTTCGAAATTGAAAGGCG
GCTTCGGCTGTCACTTAGATGGAC
CCGCGTCGCATTAGCTAGTTGGTG
AGGTAACGGCTCACCAAGGCAAC
GATGCGTAGCCGACCTGGAGGGT
GATCGGCCACACTGGGACTGAGA
CACGGCCCAGACTCCTACGGGAG
GCAGCAGTAGGGAATCTTCCGCA
ATGGACGAAAGTCTGACGGAGCA
ACGCCGCGTGAGTGATGAAGGCT
TTCGGGTCGTAAAACTCTGTTGTT
AGGGAAGAACAAGTGCTAGTTGA
ATAAGCTGGCACCTTGACGGTAC
CTAACCAGAAAGCCACGGCTAAC
TACGTGCCAGCAGCCGCGGTAAT
ACGTAGGTGGCAAGCGTTATCCG
GAATTATTGGGCGTAAAGCGCGC
GCAGGTGGTTTCTTAAGTCTGATG
TGAAAGCCCACGGCTCAACCGTG
GAGGGTCATTGGAAACTGGGAGA
CTTGAGTGCAGAAGAGGAAAGTG
GAATTCCATGTGTAGCGGTGAAA
TGCGTAGAGATATGGAGGAACAC
CAGTGGCGAAGGCGACTTTCTGG
TCTGTAACTGACACTGAGGCGCG
AAAGCGTGGGGAGCAAACAGGAT
TAGATACCCTGGTAGTCCACGCC
GTAAACGATGAGTGCTAAGTGTT
AGAGGGTTTCCGCCTTTTAGTGCT
GAAGTTAACGCATTAAGCACTCC
GCCTGGGGAGTACGGCCGCAAGG
CTGAAACTCAAAGGAATTGACGG
GGGCCCGCACAAGCGGTGGAGCA
TGTGGTTTAATTCGAAGCAACGC
GAAGAACCTTACCAGGTCTTGAC
ATCCTCTGACAACCCTAGAGATA
GGGCTTCTCCTTCGGGAGCAGAG
TGACAGGTGGTGCATGGTTGTCGT
CAGCTCGTGTCGTGAGATGTTGGT
TAAGTCCCGCAACGAGCGCAACC
CTTGATCTTAGTTGCCATCATTTA
GTTGGGCACTCTAAGGTGACTGC
CGGTGACAAACCGGAGGAAGGTG
GGGATGACGTCAAATCATCATGC
CCCTTATGACCTGGGCTACACACG
TGCTACAATGGACGGTACAAAGA

GCTGCAAGACCGCGAGGTGGAGC
TAATCTCATAAAACCGTTCTCAGT
TCGGATTGTAGGCTGCAACTCGCC
TACATGAAGCTGGAATCGCTAGT
AATCGCGGATCAGCATGCCGCGG
TGAATACGTTCCCGGGCTTTGTAC
ACACCGCCCGTCACACCACGAGA
GTTTGTAACACCCGAAGTCGGTG
GGGTAACCTTTTTGGAGCCAGCC
GCCTAAGGTGGGACAGATGATTG
GGGTGAAGTCGTAACAAGGTAGC
CGTATGGGAAGGTGT

Effects of Different Glyphosate Concentration on the Growth of Bacillus subtilis H184 and Bacillus cereus BFM4

The growth of B. subtilisH184 and B. cereusBFM4 in different concentrations of glyphosate is shown in Figure 3. The inverse relationship between the growth of B. subtilis and glyphosate shows that the herbicide is toxic to the organisms and this toxicity is concentration dependent. Thus an increase in the concentration of glyphosate brought about a corresponding decrease in the growth of the bacteria isolates for the period of 28 days. The medium containing 20 mg/ml glyphosate, mineral salt medium and B. cereus strain BFM4 was significantly ($P< 0.05$) higher, with the maximum growth of 1.38 (optical density at 482 nm) observed at day 7.

Percentage Utilization of Glyphosate

The percentage utilization in the medium containing 20 mg/ml glyphosate, mineral salt medium (MSM) and Bacillus cereus BFM4 was significantly ($P<0.05$) higher than other treatments, with maximum percentage b utilization of 97.04% at day 28 while the least percentage utilization of 2.15% was observed in the control (30 mg/ml of herbicide +MSM) (Figure 4).

Percentage Utilization of Glyphosate with Heavy Metals Using Bacillus subtilis

The percentage utilization of glyphosate with heavy metals using Bacillus subtilis H184 is shown in Figure 5. The highest percentage utilization (79.02%) of glyphosate by Bacillus subtilis was observed in the medium contaminated with 200 µg/ml Pb^{2+} at day 28, while the least percentage degradation (18.66 %) was observed in the control at day 14.

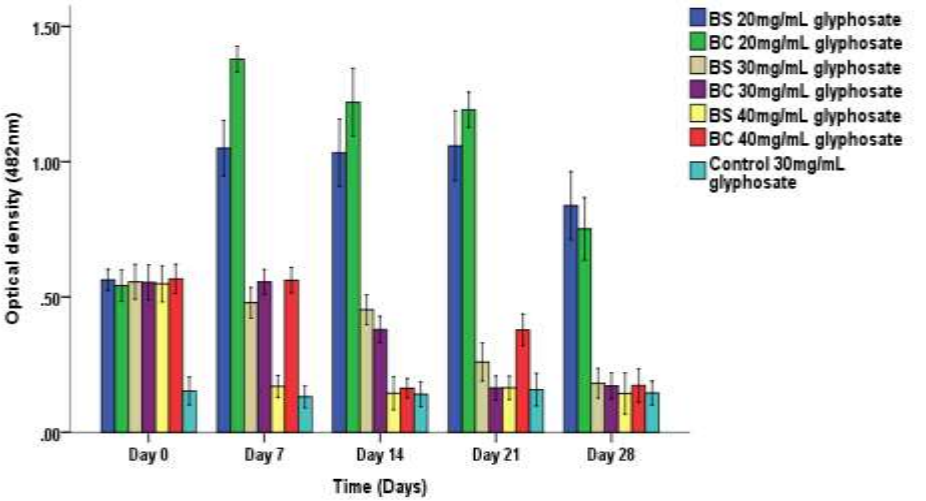

Figure 3: Effects of different glyphosate concentration on the growth of B. subtilisH184and B. cereus BFM4

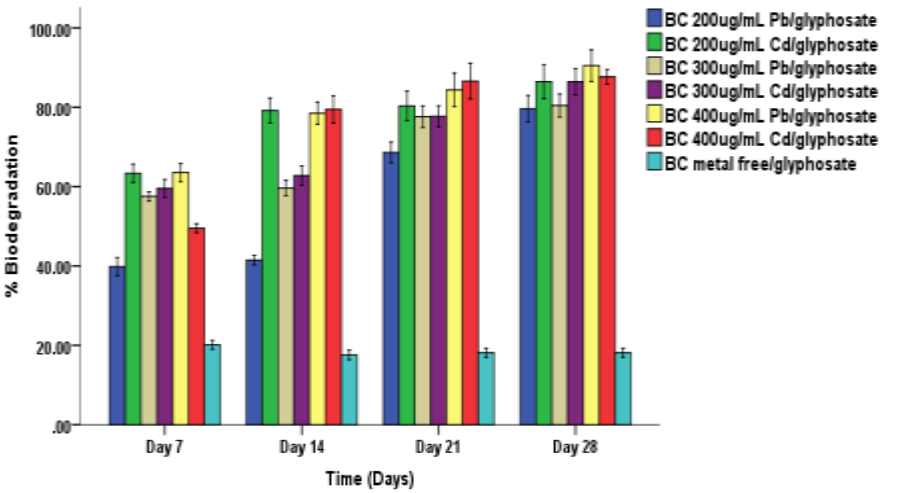

Figure 4: Percentage Utilization of Glyphosate with heavy metals using Bacillus cereusBFM4

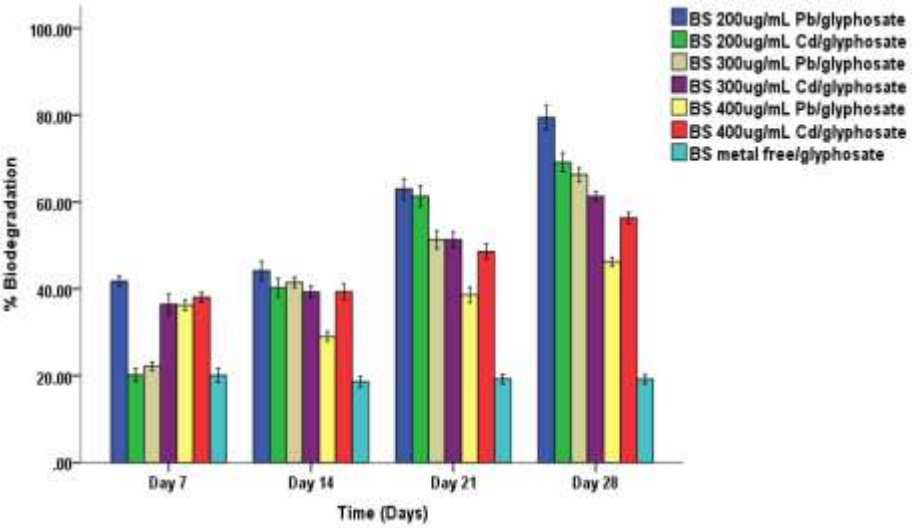

Figure 5: Percentage utilization of glyphosate with heavy metals usingBacillus subtilis H184

Bacterial Count during the Biodegradation of Glyphosate

The highest bacterial count (1.08×10^8 cfu/ml) was observed at 14 days of incubation period in the medium containing Bacillus cereus BFM4 and 20 mg/ml concentration of the herbicide while the least bacterial count (2.47×10^6 cfu/ml) was observed at day 28. The result is shown in Figure 6.

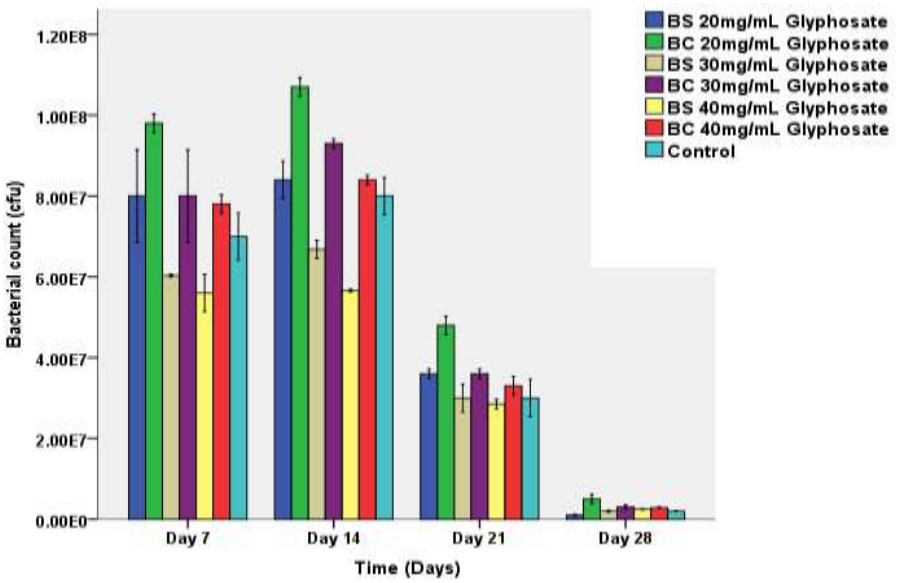

Figure 6: Bacterial Count during the Utilization of Glyphosate

Discussion

Five bacterial isolates were screened for glyphosate utilization by measuring their growth at 482 nm on medium containing glyphosate as sole phosphorous source. Of the five identified bacterial species, two (Bacillus subtilis and Bacillus cereus) were selected for further biodegradation studies based on their short lag phase and rapid utilization of glyphosate (Figure 1). E. coli, Actinomyces sp. and P. aeruginosa did not show appreciable growth as observed in Figure 1. Studies by Baboo et al. [7] showed that culturable bacteria are usually reduced in number or eliminated when extracted from soil or grown on liquid media containing glyphosate, this could be attributed to the effect due to the toxicity of the herbicide. The results in this study, which showed a reduction in the number of bacterial species grown on the glyphosate liquid medium are consistent with the report of Baboo et al. [7].

The growth of B. subtilis H184 and B. cereusBFM4 in different concentration of glyphosate gave an inverse relationship (Figure 3). The medium containing 20 mg/ml glyphosate, mineral salt medium and B. cereus BFM4 was significantly ($P< 0.05$) higher, with the maximum growth of 1.38 (optical density at 482 nm) observed at day 7 (Figure 4). This might be due to the poisonous nature of glyphosate which inhibits growth at higher concentration. This conforms to the findings of PAN International [14] who reported that glyphosate can either stimulate or inhibit soil microorganisms depending on the soil type or herbicide concentration.

The percentage utilization in the medium containing 20 mg/ml glyphosate, mineral salt medium (MSM) and Bacillus cereus BFM4 was significantly ($P< 0.05$) higher than other treatments, with maximum percentage utilization of 97.04% at day 28 (Figure 4) while the least percentage utilization of 2.15% was observed in the control (30 mg/ml of herbicide +MSM). This might be because the low concentration of the herbicide served as a substrate to the bacteria. This agrees with the findings of Huang et al.[9] who revealed that up to 20-90% of glyphosate was mineralized to CO_2 by bacteria over approximately 5 weeks, depending on the soil type.

The percentage utilization was significantly ($P < 0.05$) higher (90.49%) in the medium containing B. cereus BFM4 with herbicide contaminated with 400 µg/ml of Pb^{2+} while the least percentage utilization (18.12%) was observed in the control (metal free) as seen in Figure 5. Bacillus cereusstrain BFM4 could tolerate high heavy metal concentration. Sevim and Sevim, [15] and Adekanmbi [16] reported that heavy metal resistance in Bacillus sp. is mostly mediated by plasmids that they possess. Statistical analysis revealed that there was significant ($P< 0.05$) difference in the treatments at day 28 (Figure 5), with the medium containing B.subtilis H184 with herbicide contaminated with 200 µg/ml Pb^{2+} being significantly higher than the other treatment with a maximum percentage glyphosate utilization of 79.02 %, this could be attributed to large ionic size and heavier atomic weight of lead compared to cadmium, which enables it to have greater interaction with biological components.

This result is in line with the findings of Shameer [17] and Shamim [18] who reported that large ionic size of lead makes it to be adsorbed more than cadmium by Bacillus sp. The highest bacterial count (1.08×10^8 cfu/ml) was observed at 14 days of incubation period

in the medium containing Bacillus cereusBFM4 and 20 mg/ml of the herbicide as observed in Figure 6. The increase in bacterial count observed at day 14 in the medium containing Bacillus cereusBFM4 and 20mg/ml of the herbicide might be due to the fact that the organisms were able to utilize the herbicide as a source of nutrient for their growth and metabolism. The reduction in the bacterial count at day 21 and 28, could be attributed to the depletion of nutrients in the medium due to bacterial utilization. This is in agreement with the findings of Torretta et al. [8] who revealed that nutrient availability affects bacterial counts during biodegradation of herbicides.

Conclusion

Bacillus cereus BFM4 and Bacillus subtilis H184 were able to utilize glyphosate as sole carbon and phosphorus sources. Bacillus cereus BFM4 had higher percentage glyphosate utilization of 97.04 % in glyphosate at the lowest concentration of the herbicides. However, Bacillus cereus BFM4 had higher percentage utilization of 90.49 % in glyphosate at concentration (400 µg/ml) of the heavy metal (lead). The addition of trace amount (200 µg/ml, 300 µg/ml and 400 µg/ml) of heavy metals stimulated microbial growth, hence increasing the rate by which he glyphosate utilized the herbicides.

References

[1] Nicolas, V., Oestreicher, N. and Vélot, C. (2016) Multiple effects of a commercial roundup® formulation on the soil filamentous fungus Aspergillus nidulans at low doses: evidence of an unexpected impact on energetic metabolism, Environ Sci. Pollut. R., 10(3), 1-12.

[2] Kanissery, R.G., Welsh, A. and Sims, G.K. (2015) Effect of soil aeration and phosphate addition on the microbial bioavailability of carbon-14-glyphosate, J. Environ. *Qual*., 12(4), 213-225.

[3] Zablotowicz, R. M, Krutz, L. J, Weaver, M. A, Accinelli, C, and Reddy, K. N. (2008) Glufosi-nate and ammonium sulfate inhibit atrazine degradation in adapted soils. Biol Fert Soils, 45(1), 19-26.

[4] Goda, S.K., Elsayed, I.E., Khodair, T.A., El-Sayed, W. and Mohamed, M.E. (2010) Screening for and isolation and identification of malathion-degrading bacteria: cloning and sequencing a gene that potentially encodes the malathion-degrading enzyme, carboxylestrase in soil bacteria. Biodegradation, 21(3), 903-913.

[5] Todorovic, G.R., Rampazzo, N., Mentler, A., Blum, W.E.H., Eder, A. and Strauss, P. (2014) Influence of soil tillage and erosion on the dispersion of glyphosate and aminomethylphosphonic acid in agricultural soils, Int. *Agrophys* 28(10), 93 –100.

[6] Benbrook C. M. (2016) Trends in glyphosate herbicide use in the United States and globally, Environ Sci Eur 28(1), 3. doi:10.1186/s12302-016-0070-0

[7] Baboo, M., Pasayat, M., Samal, A., Kujur, M., Maharana J.K. and Patel, A.K. (2013) Effect of four herbicides on soil organic carbon, microbial biomass-c, enzyme activity and microbial populations in agricultural soil, Int J Environ Sci Te 3(4), 100-112.

[8] Torretta, V., Katsoyiannis , I.A., Viotti, P. and Rada, E.C. (2018) Critical review of the effects of glyphosate exposure to the environment and humans through the food supply chain. Sustainability, 10, 950; doi:10.3390/su10040950

[9] Huang, Y., Xiao, L., Li, F., Xiao, M., Lin, D., Long, X., and Wu, Z. (2018) Microbial degradation of pesticide residues and an emphasis on the degradation of cypermethrin and 3-phenoxy benzoic acid: a review. Molecules (Basel, Switzerland), 23(9),2313. doi:10.3390/molecules23092313

[10] Kanissery, R.G., Welshb, A. and Sims, G. K. (2015) Effect of soil aeration and phosphate addition on 368 the microbial bioavailability of carbon-14-glyphosate. J. Environ. Qual. 44, 137-144. doi:369 10.2134/jeq2014.08.0331

[11] Dadrasnia, A. and Agamuthu, P. (2010) Enhanced degradation of diesel-contaminated soil using organic wastes, MJS 29(3), 225-230

[12] Cheesbrough, M. (2006) District Laboratory Practice in Tropical Countries, 2006. Part 2, Cambridge University, Press U.K, 325.

[13] Moneke, A.N., Okpala, G.N. and Anyanwu, C.U. (2010) Biodegradation of glyphosate herbicide in vitro using bacterial isolates from four rice fields. Afr. J. Biotechnol., 9(26), 4067-4074.

[14] PAN International (2017) Pesticide Action Network - Glyphosate monograph. Retrieved from https://issuu.com/pan-uk/docs/glyphosate_monograph_complete

[15] Sevim, A. and Sevim, E. (2015). Plasmid mediated antibiotic and heavy metal resistance in Bacillus strains isolated from soils in rize, Turkey. J. Nat. Appl. Sci 19(2), 133-141.

[16] Adekanmbi, A.O., Adelowo, O.O., Okoh, A.I. and Fagade, O.E. (2019) Metal-resistance encoding gene-fingerprints in some bacteria isolated from wastewaters of selected printeries in Ibadan, South-western Nigeria, Journal of Taibah University for Science, 13(1), 266-273, doi: 10.1080/16583655.2018.1561968

[17] Shameer, S. (2016) Biosorption of lead, copper and cadmium using the extracellular polysaccharides (EPS) of *Bacillus* sp., from solar

salterns. 3 Biotech 6: 194. https://doi.org/10.1007/s13205-016-0498-3

[18] Shamim, S. (2018) Biosorption of Heavy Metals, Biosorption, Jan Derco and Branislav Vrana, IntechOpen, DOI: 10.5772/intechopen.72099. Retrieved from: https://www.intechopen.com/books/biosorption/biosorption-of-heavy-metals

Covenant Journal of Physical & Life Sciences (CJPL) Vol. 7 No. 2. Dec. 2019
ISSN: ***p. 2354 – 3574 e. 2354 – 3485*** **DOI:**

An Open Access Journal Available Online

Performance Enhancement in Cellular Network Using Decoding-based Successive Interference Cancellation Technique

Kingsley Eghonghon Ukhurebor[1] * & Wilson Nwankwo[2]

[1]Climatic/Environmental/Telecommunication Physics Unit, Department of Physics, Edo University Iyamho, P.M.B. 04 Auchi, Edo State, Nigeria
[2] Software Engineering/Cyber Physical Lab, Department of Computer Science, Faculty of Science, Edo University Iyamho, P.M.B. 04 Auchi, Edo State, Nigeria
*ukeghonghon@gmail.com; ukhurebor.kingsley@edouniversity.edu.ng

Received: xxxx xxxxxx, 2019 Accepted: xxxx xxxxxx,, 2019
Date of Publication: December, 2019

Abstract: Interference if not properly attended to could have negative influence on the air interface performance of any wireless network service. Hence, there is a need to moderate interference in cellular network system. This study is aimed at analysing the performance of decoding-based successive interference cancellation technique. The was done analysing the performance of decoding based successive interference cancellation on uplink High Speed Uplink Packet Access Enhanced Dedicated Physical Data Channel. From the analysis, simulations and results obtained from this study, we have been able to show that this technique would reduce the load of the cell and increase the network capacity of the cellular network provider, thereby improving the quality of service.
Keywords: Cellular Network; Quality of Service; Performance; Interference; Uplink

Introduction

Since the development of mobile telecommunication, the industries have undergone great changes and seen momentous advancements. The mobile telecommunication industries which are involved in wireless networks provision have changed from making marginal

military and vehicle-oriented products to delivering mobiles and network components to mass markets [1-5].

According to [6], "to have a better communication link for radio wave, the transmission medium needs to be considered in order to have a better signal from the radio communication network, since the radio wave communication links are influenced by meteorological variables". The attitude and phase scintillations, absorption, scattering of radio wave network signals and other numerous complex mechanisms that occur in the troposphere are caused by the random changes in the surface and vertical refractivity which can cause transmission signals lost and co-channel interference [7-10]. The consequence of interference as a result of refractivity difference in the troposphere is much in the humid climate than in the temperate climate regions due to the occurrence of high intensity humid rainfall [6-7].

Signal interference in wireless networks negatively affects transmission coverage and mobile capacity, limiting overall network performance, especially in the uplink. Unavoidable signal interference is becoming more prevalent in wireless networks with the increasing numbers of active transmitters on the Radio Frequency (RF) spectrum. In wireless network, interference can affect the transmission of the mobile to the cell site (Uplink) as well as the transmission of the cell site to the mobile (Downlink). It is however, to note that the uplink is mostly affected by interference due to the fact that the cell sites have higher levels of power transmission [1, 11].

Interference analysis in wireless network has three main stages:

(i) Detection; which have to do with using metrics that monitor the spectrum activity in frequency and time domain allowing continuous recording of spectrum analysis and spectrogram measurements.

(ii) Identification; having the ability to identify the type of interference signal through demodulation.

(iii) Location; performing directional measurements, recording the geographical coordinates used to triangulate and find the intersection area which represent the geographical location of the interferer [1, 11].

During the initial development of wireless cellular networks, the second generation (2G) cellular wireless networks produce much interference. However, the interference from the third generation (3G) wireless cellular networks is considerably lower than the ones from the 2G networks. Wideband code division multiple access (WCDMA) system; third-generation mobile systems are gradually being deployed in many developing countries like Nigeria in hotspot areas. However, owing to the number of new infrastructures require and the economical situations on ground in some of these countries, it is now that 3G are becoming prevalent, especially in remote villages in these developing countries [1, 2].

In Release 5, High Speed Downlink Packet Access (HSDPA) technology was introduced. This greatly increased

downlink transmission rate. In order to meet the rapidly growing demands for data services in the uplink, the 3rd Generation Partnership Project (3GPP) Release 6 introduced High Speed Uplink Packet Access (HSUPA). The technical advancements in HSUPA include fast scheduling, Fast Hybrid Automatic Repeat Request (HARQ), shorter Transmission Time Interval (TTI), and macro diversity combining (MDC).

The benefits of HSUPA were improvement in the uplink capacity, increase in user data rate, and reduction in the transmission delay on the WCDMA network.

HSUPA has the following impacts on the network:

(i) A new control channel that requires more power in the uplink, called Enhanced Dedicated Physical Control Channel (E-DPCCH).

(ii) When the uplink load is limited and there is a large number of User Equipment (UEs). The UEs can upload data only at a guaranteed bit rate (GBR), for example, 64 kbit/s. As compared with R99 channels, E-DPCCH consumes more system resources.

HSUPA Physical Channels is shown in Figure 1.

The Enhanced Dedicated Channel (E-DCH) has a TTI of either 10 ms or 2 ms. It is mapped onto the Enhanced Dedicated Physical Data Channel (E-DPDCH) or E-DPCCH. When the transmission time interval (TTI) is 10 ms, the Enhanced Dedicated Channel (E-DCH) provides better uplink coverage performance but when the TTI is 2 ms, the E-DCH provides higher transmission rates.

The E-DPDCH carries data in the uplink. The spreading factor of the E-DPDCH varies from SF256 to SF2 depending on the data transmission rate.

The E-DPCCH carries control information related to data transmission in the uplink. The control information consists of the E-DCH Transport Format Combination Indicator (E-TFCI), Retransmission Sequence Number (RSN), and happy bit. The SF of the E-DPCCH is fixed to 256.

To implement the hybrid, acknowledge repeat request (HARQ) function, the Enhance HARQ Indicator Channel (E-HICH) is introduced in the downlink. The E-HICH carries retransmission requests from the NodeB. The SF of the E-HICH is fixed to 128.

The downlink Enhanced Access Grant Channels (E-AGCH) and Enhanced Relative Grant Channel (E-RGCH) carry the HSUPA scheduling control information. The E-AGCH is a shared channel, which carries the maximum E-DPDCH to DPCCH power ratio, that is, absolute grants. The SF of the E-AGCH is fixed to 256.

The E-RGCH is a dedicated channel, which is used to indicate relative grants and increase or decrease the maximum E-DPDCH to DPCCH power ratio. The SF of the E-RGCH is fixed to 128 [12, 13].

This study is aimed at analysing the performance of decoding-based successive interference cancellation technique whose functions are as follows:

(i) The Network detects and decodes E-DPDCH signals from HSUPA UEs.
(ii) Network regenerates signals of UEs on their respective E-DPDCHs by using the detection results and channel estimation results.
(iii) The regenerated signals are then removed from the received signals before detection for demodulation.
(iv) The Network processes the signals of another HSUPA UE and the process continues.

Methodology

It is becoming obvious that modern-day wireless network systems are gradually interference restricted. There is an ascending interest in using advanced/unconventional interference mitigation techniques for the improvement of cellular network performance as well as the conventional techniques of mitigating interference as contextual noise [13-17].

According to [13], one of the most important method is successive interference cancellation. Though, successive interference cancellation is not always the best multiple access scheme in wireless network systems, it is specifically open to execution and does accomplish restrictions of the dimensions regions in multiuser systems in many cases [13]. Conventional performance analyses of successive interference cancellation do not consider the spatial distribution of the users.

The transmitters are either presumed to exist at a given location with deterministic path loss and the references within, or presumed subject to centralized power control which to a large extent recompenses for the channel unpredictability [17].

In launching the advanced/unconventional models, spatial distribution of the users, is essentially taken into consideration [13].

Successive Interference Cancellation Model and Metrics

According to [13], if we are considering a situation where all the users transmit with unit power, it is appropriate to introduce the following standard signal-to-interference ratio based single user decoding condition:

Standard Signal-to-Interference Ratio Based Single User Decoding Condition

In an interference-limited network, a particular user at $x \in \Phi$ can be successfully decoded without successive interference cancellation, if only:

$$SIR_x = \frac{h_x \| x \|^{-\alpha}}{\sum_{y \in \mathbf{\Phi}} h_x \| y \|^{-\alpha}} \succ \theta \quad (1)$$

Where SIR_x is the standard signal-to-interference ratio based single user, $h_x \| x \|^{-\alpha}$ is the received signal power from x, $\sum_{y \in \mathbf{\Phi}} hy \| y \|^{-\alpha}$ is the aggregate interference from the other active transmitters and θ is the standard signal-to-interference ratio based decoding threshold.

Similarly, in a situation of perfect interference cancellation, once a user is successfully decoded, its signal component can be completely subtracted from the received signal.

Assuming the decoding order is always from the stronger users to the weaker users, we obtain the following decoding condition for the case with signal-to-interference ratio [13].

Signal-to-Residual-Interference Ratio-Based Decoding Condition with Successive Interference Cancellation.

With successive interference cancellation, a user x can be decoded if all the users in $\tau_c = \left\{ y \in \mathbf{\Phi} : h_x \left\| y \right\|^{-\alpha} \succ h_x \left\| x \right\|^{-\alpha} \right\}$ are successfully decoded and the signal-to-residual-interference ratio at *x*.

$$SIR_x = \frac{h_x \left\| x \right\|^{-\alpha}}{\sum_{y \in \mathbf{\Phi} \setminus \{x\} \setminus \tau_c} h_y \left\| y \right\|^{-\alpha}} \succ \theta \quad (2)$$

Consequently, consider the ordering of all nodes in Φ such that $h_{xi} \left\| x_i \right\|^{-\alpha} \succ h_{xj} \left\| x_j \right\|^{-\alpha}, \forall_i \prec j^5$. The number of users that can be successively decoded is N if only:

$$h_{xi} \left\| x_i \right\|^{-\alpha} \succ \theta \sum_{j=i+1}^{\infty} h_{xj} \left\| x_j \right\|^{-\alpha}, \forall_i \leq N$$

and

$$h_{xN+1} \left\| x_{N+1} \right\|^{-\alpha} \leq \theta \sum_{j=N+1}^{\infty} h_{xj} \left\| x_j \right\|^{-\alpha}.$$

It is noteworthy, according to [13], "that the received power ordering is only presented for analysis purposes. As is not necessary, we do not assume that the received power ordering is known a priori at the receiver".

According to [13], the mean number of users that can be successively decoded; E[N], with respect to different system parameters and the distribution of N in the form:

$$P_k \underset{=}{\Delta} \mathrm{P}\left(N \geq k \right) \quad (3)$$

Eqn. (3) is known as the probability of successively decoding at least k users at the origin. To make the dependence on the point process clear, occasionally we have to use $P_k(\Phi)$.

Since successive interference cancellation is intrinsically a multiple packet reception (MPR) scheme, we can further define the aggregate sum rate (throughput) to be the total information rate received at the receiver o, because all the users in the system transmit at the same rate log (1 + θ), the sum rate is:

$$R = \mathrm{E}\left[\log(1+\theta) N \right] = l \log(1+\theta) \mathrm{E}\left[N \right] \quad (4)$$

In this study, the evaluation of the gains from decoding-based successive interference cancellation technique would be noticeable when HSUPA 2 ms TTI UEs with continuous data transmission account for a larger proportion of total UEs in a cell or when HSUPA 2 ms TTI UEs with high throughput/sum rate exist in a cell. This would amount to high Uu-interference load.

Discussion of Results

The number of Dedicated Channel (DCH) UE's as compared to UL load of different cells is shown in Figure 2. It is observed from this figure that there is a great gain in DCH UEs Vs Receive Total Wideband Power (RTWP) distribution for high number of users. It can be seen from the above chart showing DCH User number Vs RTWP trend that post RTWP samples have shifted to lower values particularly on

cells with DCH UE numbers greater than 60. This is a great achievement as for cells with high user numbers, whose experience was supposedly very poor as a result of high RTWP were greatly improved.

The number of TTIs in which HSUPA users transmit data under different air interface loads in a cell (X=3, 6, 7, 9, 10, 13, 20) is shown in Figure 3. From the figure is it noticed that there is a great improvement between cell loads of 6dB to 10dB range.

The number of HSUPA users with data transmission under different uplink Uu interface loads in a cell (X=3, 6, 7, 9, 10, 13, 20) is shown in Figure 4. The figure reveals the number of HSUPA users with data transmission at different load ranges in the air interface. There was also a great improvement is observed at 6dB to 10dB range, with the system maintaining stability at 13dB range.

The number of times that cell Uu-interface load is between Ydb to Zdb; Ratio of the Actual RTWP in a cell to the Reference RTWP, (X=0~25) is shown in Figure 5.

The figure reveals the uplink load distribution comparison before and after the study. It was observed that the trend is stable with no major gain in the load distribution. This could be attributed to low number of users processed during the course of the study.

Conclusion

From the analysis, simulations and results obtained from this study, we have been able to show that this technique would reduce the load of the cell and increase the network capacity of the cellular network provider, thereby improving the quality of service.

It is therefore recommended that cellular network service providers should adapt this technique in mitigating interference in WCDMA so as to implore and optimize the quality of service generally.

Acknowledgments

Gratitude to Associate Prof. Wilson Nwankwo, Ph.D. who assisted in attending to the reviewer's comments and improving the article generally.

References

[1] Ukhurebor, K.E., Moses Maor, M.S. and Aigbe, E.E. (2017) Mollification of WCDMA Interference on Uplink Channels in Cellular Network Using the Power Control Approach, BJAST, 20(4), 1-11.

[2] Lawal, B.Y., Ukhurebor, K.E., Adekoya, M.A. and Aigbe E.E. (2016) Quality of Service and Performance Analysis of A GSM Network in Eagle Square, Abuja and Its Environs, Nigeria, IJSER, 7(8), 1992- 1999.

[3] Ukhurebor, K.E. and Aigbe, E.E. (2016) Evaluating Pathloss Propagation Using Okumura-Hata Model for Surulere Area in Lagos State, Nigeria, Journal of NAMP, 36(2), 291-296.

[4] Ukhurebor, K.E., Andikara, J. and Azi, S.O. (2015) Effects of Upsurge of Human Traffic on the Quality of Service of GSM Network in Eagle Square Abuja, Nigeria, IJSER, 6(11), 89- 104.

[5] Ukhurebor, K.E., Awodu, O.M., Abiodun, I.C. and Azi, S.O. (2015) A Comparative Study of the Quality of Service of GSM Network during Crowd Upsurge in University of Benin, Nigeria, IJSER, 6(10), 1484- 1497.

[6] Ukhurebor, K.E. and Odesanya I. (2019) Relationship between Meteorological Variables and Effective Earth Radius Factor over Auchi, Edo State, South-South, Nigeria, CJPL (SE), 7(1), 1-10.

[7] Ukhurebor, K.E., Azi, S.O., Abiodun, I.C. and Ojiemudia, S.E. (2018) The Influence of Weather Variables on Atmospheric Refractivity over Auchi, South-South, Nigeria, J. Appl. Sci. Environ. Manage., 22(4), 471-475.

[8] Ukhurebor, K.E. and Azi, S.O. (2019) Review of Methodology to Obtain Parameters for Radio Wave Propagation at Low Altitudes from Meteorological Data: New Results for Auchi Area in Edo State, Nigeria, Journal of King Saud University – Science, 31(4), 1445–1451.

[9] Ukhurebor, K.E. and Umukoro, O.J (2018) Influence of Meteorological Variables on UHF Radio Signal: Recent Findings for EBS, Benin City, South-South, Nigeria, IOP Conf. Ser.: Earth Environ. Sci., 173, 012017.

[10] Ukhurebor, K.E., Olayinka, S.A., Nwankwo, W. and Alhasan, C. (2019) Evaluation of the Effects of some Weather Variables on UHF and VHF Receivers within Benin City, South-South Region of Nigeria, J. Phys.: Conf. Ser., 1299, 012052.

[11] Hult, T., Grace, D. and Mohammed, A. (2008) WCDMA Uplink Interference Assessment from Multiple High-Altitude Platform Configurations, EURASIP Journal on Wireless Communications and Networking, 2008, 1-7.

[12] Application Note: Radio Access Network Interference Analysis. (2012)
JDS Uniphase Corporation.

[12] 3GPP TS 25.321. V4.10.0. (2004) 3rd Generation Partnership Project; Technical Specification Group Radio Access Network, Medium Access Control (MAC) protocol specification, 3GPP Organizational Partners (ARIB, ATIS, CCSA, ETSI, TTA, TTC).

[13] Zhang, X. and Haenggi, M. (2014) The Performance of Successive Interference Cancellation in Random Wireless Networks, IEEE Global Telecommunications, 2014, 1-50.

[14] Miridakis, N. and Vergados, D. (2012) A Survey on the Successive Interference Cancellation Performance for Single-Antenna and Multiple-Antenna OFDM Systems, IEEE Communications Surveys & Tutorials, 15(99), 1–24.

[15] Damnjanovic, A., Montojo, J., Wei, Y., Ji, T., Luo, T., Vajapeyam, M., Yoo, T., Song, O. and Malladi, D. (2011) A Survey on 3GPP Heterogeneous Networks,

IEEE Wireless Communications, 18(3), 10–21.

[16] Lopez-Perez, D., Guvenc, I., Roche, D., Kountouris, M., Quek, T. and Zhang, J. (2011) Enhanced Intercell Interference Coordination Challenges in Heterogeneous Networks, IEEE Wireless Communications, 8(3), 22–30.

[17] Weber, S., Andrews, J., Yang, X. and Veciana, G.D. (2007) Transmission Capacity of Wireless Ad-hoc Networks with Successive Interference Cancellation, IEEE Transactions on Information Theory, 3(8), 2799–2814.

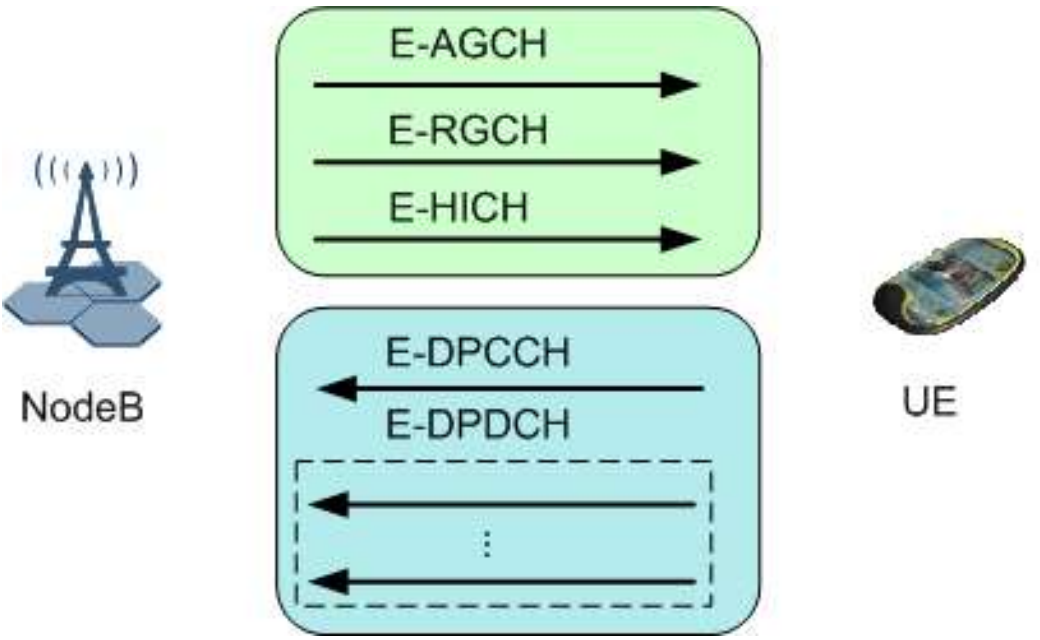

Figure 1: HSUPA Physical Channels

Figure 2: Number of DCH UE's as Compared to UL Load of Different Cells

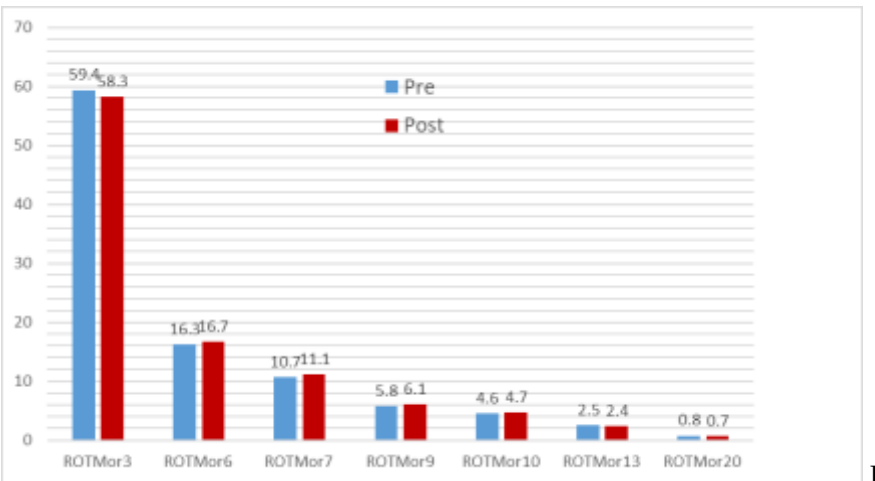

Figure 3: Number of TTIs in which HSUPA Users Transmit Data under Different air Interface Loads in a Cell (X=3, 6, 7, 9, 10, 13, 20)

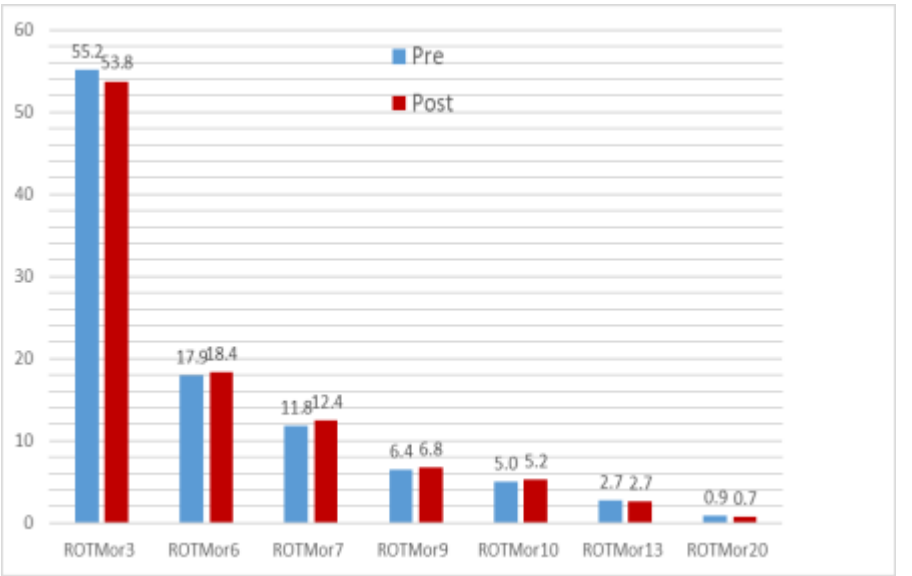

Figure 4: Number of HSUPA Users with Data Transmission under Different Uplink Uu Interface Loads in a Cell (X=3, 6, 7, 9, 10, 13, 20)

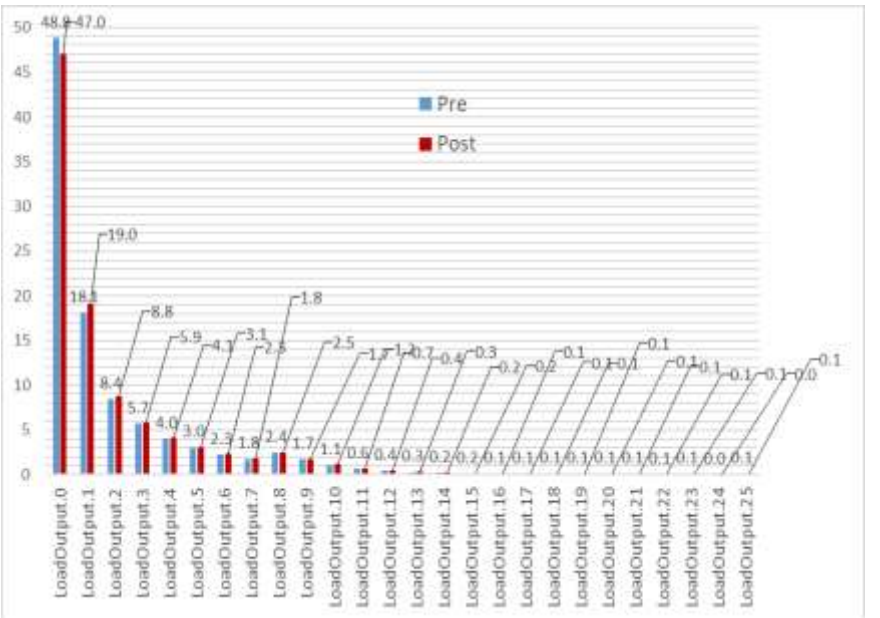

Figure 5: Number of times that Cell Uu-lnterface Load is between Ydb to Zdb; Ratio of the Actual RTWP in a Cell to the Reference RTWP, (X=0~25)

Covenant Journal of Physical & Life Sciences (CJPL) Vol. 7 No. 2, Dec. 2019
ISSN: ***p. 2354 – 3574 e. 2354 – 3485*** **DOI:**

An Open Access Journal Available Online

Isolation of Bacterial Species Capable of Producing Polyhydroxyalkanoate

Akinmulewo Adebola B. [1*] **& Nwinyi Obinna C.** [1]

[1]Department of Biological Sciences, Covenant University,

Ota, Ogun State, Nigeria.

*adebola.akinmulewo@stu.cu.edu.ng

Received: xxxx xxxxxx, 2019 Accepted: xxxx xxxxxx,, 2019
Date of Publication: December, 2019

Abstract: The major threat posed by petroleum-based plastics is environmental pollution, which further leads to death of marine animals from the plastic toxicity. A continuous scientific research on plastic innovations would help solve the plastic menace. Hence, this study was carried out to isolate and characterize microbial strains from high organic deposit sites capable of polyhydroxyalkanoate (PHA) production. Samples of soil and organic wastes were collected from Olusosun dumpsite, Ojota, motor mechanic shop at Covenant University, Ota and kitchen sewage from Covenant University's Cafeteria 2. Twenty bacterial isolates were obtained and screened for the ability to utilize waste frying oil and cassava effluent as cheap carbon substrates to synthesize PHA polymers. Quantitative analysis was carried out after 72 hours by crotonic assay method using the UV spectrophotometer at 235 nm wavelength. The result showed that there is no significant difference ($p<0.05$) between the PHA accumulated when either substrates are utilized by the isolates. The quantitative analysis result for the identification of monomeric units of PHA using Gas chromatography-mass spectrometry showed four isolates with capacities to yield more PHAs than other isolates under the subjected growth condition. These four isolates selected were characterized, morphological and phylogenetic characterization results showed

that all four isolates A1 (MK989593), A2 (MK989594), A4 (MK989595), A6 (MK989596) have similarity (>90%) to the *Alcaligenes* spp. respectively. The use of waste oils and cassava effluent to produce PHAs by isolates used in this study can be considered good candidates for cheap substrates choices to further optimize PHA production industrially.

Keywords: Polyhydroxyalkanoate, Biopolymers, Crotonic acid, Waste frying oil, Cassava effluent

Introduction

Despite the wide range of application, plastics are non-biodegradable and therefore end up as waste litters with high staying power [1, 2, 3]. Synthetic plastics don't biodegrade [4], because they resist corrosion, they rather undergo fragmentation during photo-oxidation forming microplastics and nanoplastics [5, 6]. The accumulation on land creates pyramids of waste extending to the marine environment by various dispersal mechanism leading to disruption of the aquatic habitat [2, 7, 8, 9].

Putting into consideration endangered species of the marine habitat as well as a possible disruption of man's food chain through consumption of toxic sea products; there is the urgent need to reduce the impact of plastic pollution.

Polyhydroxyalkanoates (PHA) have been proposed as substitutes for petroleum-based synthetic polymers due to their biodegradability and biocompatibility [10]. It has been estimated that at least 30% or more of PHA cost is attributed to carbon, nutrients and aeration cost, thus, PHA is not cost competitive compared to fossil-derived products. The cost of synthetic plastics ranges between US$0.60-0.87/lb, while the cost of PHA production ranges between US$2.25-2.75/lb, the cost of commercially producing PHA is higher as opposed to synthetic plastics and not cost effective [11]. According to [12, 13], there is need for continuous scientific research for new innovations that would tackle the plastics menace, through exploration of microbial plastics as an alternative to the conventional synthetic plastics. Therefore, this study was aimed at utilizing cheap and sustainable carbon source to produce polyhydroxyalkanoate (PHA) as an alternative to the synthetic plastics

Materials and Methods

Sample collection

The isolates used for this research were isolated from four sources. Organisms were isolated from soils at Olusosun dumpsite, Ojota within latitude 6.591N to 6.594N and longitude3.372E to 3.377E, motor mechanic shop at Covenant University, Ota within latititude 6.673 N to 6.674N and longitude 3.162E to 3.163E and kitchen sewage from Covenant University's Cafeteria 2 within latititude 6.6735 N to 6.6736N and longitude 3.1621E to 3.1623E The carbon sources: cassava effluent, were obtained from Sango-ota market, Ogun state and waste-frying oil from Covenant University's Cafeteria 2. The soil samples were collected using a hand trowel and placed in a sterile sampling bag and then transported to the microbiology laboratory at Covenant University for further analysis.

Enrichment and Isolation of Pure Bacteria Culture

Five grams (5 g) of each sample was sieved using a sieve with a woven wire mesh and dispensed into 250 ml conical flask in triplicates containing 100 ml Minimal salt medium [10]. This was homogenized by gently stirring to allow soil to evenly spread and mix with the medium. Aliquots of the cassava effluent and waste frying oil were added to supplement as carbon and energy source. The bioreactor was incubated in a mechanical shaker for 5 days at 30^0C. Following the end of the incubation period, 0.1 ml of the enrichment broth was pipette into nutrient agar medium by spread plate method, and then plates were incubated at 37^0C for 24 hours. The isolated colonies were sub-cultured again by streaking method on nutrient agar plates, incubated at 37^0C for 24 hours. The pure cultures obtained were maintained at 4^0C on nutrient agar slants. The cultures were maintained by sub-culturing once in 6 weeks.

PHA accumulation experiment using cheap substrates

Prior to the PHA accumulation experiment, the cells were grown in nutrient broth for 18 – 24 hrs and centrifuged afterwards at 4000 rpm for 20 minutes. Harvested cell pellets for each experiment was inoculated into 100 ml of nutrient limiting minimal salt medium in a 250 ml conical flask. 50 ml of carbon source were added to each flask. The pure isolates obtained were grown in different carbon source; in medium containing cassava effluent as excess carbon source and in medium containing waste frying oil. The culture was incubated in a mechanical shaker at 30^0C for 72 hours at 150 rpm. Aerobic conditions were constantly monitored. The optical density (600 nm) was measured at time 0 and 72 hour respectively.

Extraction of PHA

The polymer was extracted after 72 hours of culture. Extracted by treatment with several solvents as described by [14]. After 72 h of incubation at 37°C culture broth was centrifuged at 8000 rpm for 15 min. The pellet along with 10 ml sodium hypochlorite was incubated at 50°C for 1 h for lyses of cells. The cell extract obtained was centrifuged at 12000 rpm for 30 min and then washed sequentially with distilled water, acetone, and absolute ethanol. After washing, the pellet was dissolved in 10 ml chloroform (AR grade) and incubated overnight at 50°C and was evaporated at room temperature.

Quantitative analysis of PHA by crotonic assay

The extracted polymer was dissolved in 10 ml Sulphuric acid and allowed to boil at 100^0C for 10 minutes as described by [14]. In the presence of PHA, Crotonic acid would be formed afterwards. Crotonic acid gives maximum absorbance at 235 nm when measured with UV spectrophotometer. The amount of Crotonic acid was calculated from the molar extinction coefficient which is 1.55×10^4 as described by [15]. The concentration of the PHA extracted from the bacteria isolates was determined using the beer lambert law.

Data Analysis

Microsoft excel was used to calculate for T-Test for the statistically significant

values. A P-value below 0.05 was considered significant.

Microscopic and Biochemical characterisation of pure isolates

Four isolates were selected based on the concentration of PHA accumulated from the enrichment experiment. They were characterised based on cultural and morphological differences. They were analysed further using biochemical tests which includes; catalase tests, oxidase test, indole, spore test, Vogues-Proskauer, methyl red, sugar utilisation, citrate and starch hydrolysis.

Molecular characterisation of bacteria isolates

The isolates A1, A2, A4 and A6 were cultivated in nutrient broth for 24 h at 30^0C. Cells were harvested by 15 min centrifugation at 12,000 rpm and their genomic DNA was extracted using the DNA extraction protocol by [16]. The 16S rRNA gene was amplified by PCR using the universal primers for prokaryotes 907R (5'-CCGTCAATTCMTTTRAGTTT-3') and 1492R (5'TACGGYTACCTTGTTACGACTT-3'). The 16S rRNA gene sequencing using the Sanger method was carried out on ABI 3500XL Genetic Analyzer, POP7TM (ThermoScientific). The sequences were trimmed on the Geneious Prime software and compared with previously published sequences of bacterial strains using the BLAST command available on the National Center for Biotechnology Information (NCBI) database. Obtained sequences were trimmed and then compared against other sequences in the NCBI Genbank database using the BLAST program. Multiple alignments were performed using the Geneious algorithm, phylogenetic trees were built using the Neighbor Joining method [17]. All sequence analysis was conducted in Geneious 2019.1.3.

Polymer analysis using GCMS

For molecular analysis of the produced polymer, quantitative analysis was carried out on the dried extracted cell pellets. As described by [18], the cells were treated with a mixture of 0.2 ml chloroform, 1.7 ml methanol and 0.3 ml of 98% Sulphuric acid. The lower organic layer of hydroxyalkanoate (HA) was used for GC/MS analysis. The samples were injected in the splitless mode utilizing helium (He) as the carrier gas. The program cycle was at an initial temperature of 60 °C which was held for 1 min, then oven was ramped 4 °C/min to 110 °C. Oven was held for 3 mins and ramped to 260°C at 8 °C/min. Oven was then held for 5 mins and then ramped to 300°C at 10 °C/min, this was then held for 12 min. the total run time was 56.25 min. The mass spectra obtained were compared with the NIST-14 library.

Results and Discussion

Isolation of Bacteria and PHA accumulation experiment using cheap substrates Nwinyi and Owolabireported that utilizing molasses as carbon source under enrichment experiment, enabled the selection of competent organisms capable of producing PHA. In this study, the enrichment experiment was therefore used to isolate the bacterial species capable of utilizing waste frying oil and cassava effluent as the selected carbon source. From the enrichment culture, ten (10) pure bacteria isolates

were isolated successfully. The optical density (OD) taken at time 0 hr and 72 hr as shown in Fig. 3.1 and Fig. 3.2 proved the organisms were able to utilize the carbon sources leading to increase biomass. During this phase, the isolates utilised their respective carbon substrates in a nitrogen-limiting salt medium.

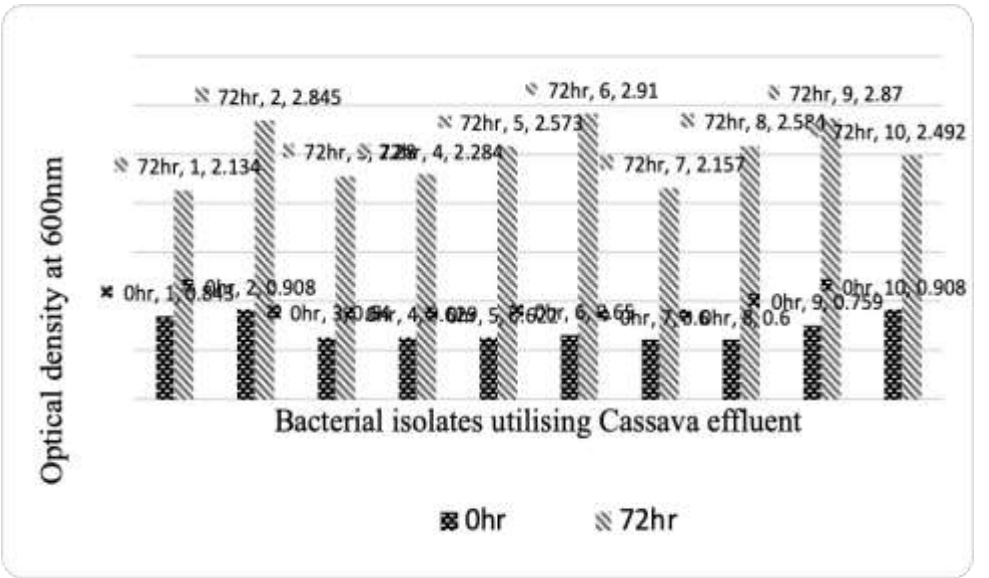

Fig 3.1: Optical densities of bacterial isolates against time measured at 600 nm during PHA accumulation phase utilizing excess cassava effluent as carbon source in a nitrogen-limiting medium

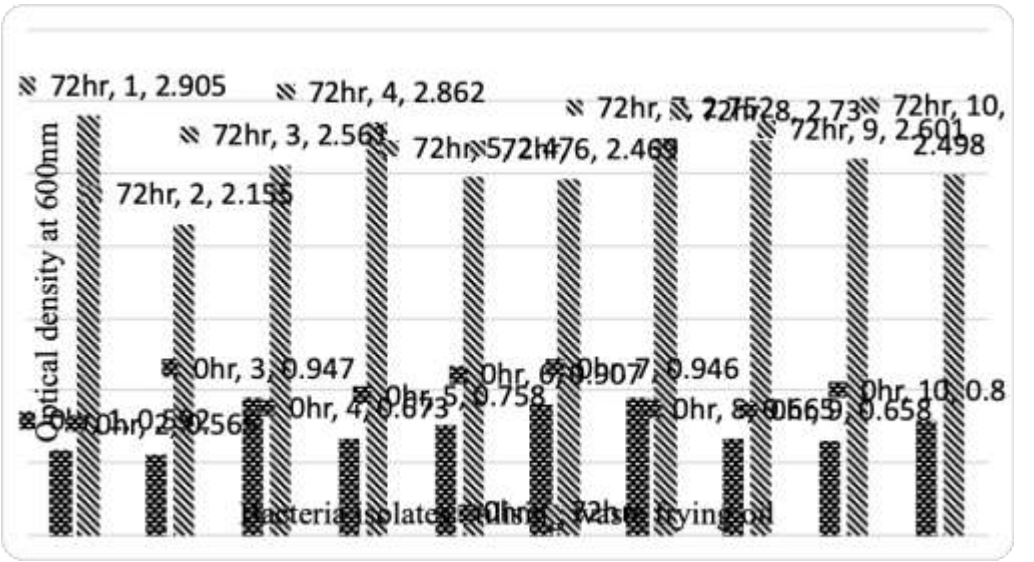

Fig 3.2: Optical densities of bacterial isolates against time during PHA accumulation phase utilizing excess waste frying oil as carbon source in a nitrogen-limiting medium

PHA extraction and quantification of PHA by Crotonic assay method

Although staining and genetic methods have been used to primarily detect the presence of intracellular PHA in organisms, they have not proven to successfully quantify PHA and give no information about the monomeric composition [19]. This study aimed at quantifying the PHA polymer after production. The Crotonic assay method has proven to be a reliable and convenient method to quantify PHAs extracted from microorganisms [15]. PHAs are converted into Crotonic acid in the presence of concentrated Sulphuric acid. Crotonic acid gave a maximum absorbance at 235 nm using the UV spectrophotometer. This procedure was described by [14]. At wavelength 235 nm, the absorbance of Crotonic acid from each isolate was read. According to beer lambert law, absorbance values are linear to the concentration. Fig 3.3 shows the different absorbance value which indicated PHA concentration.

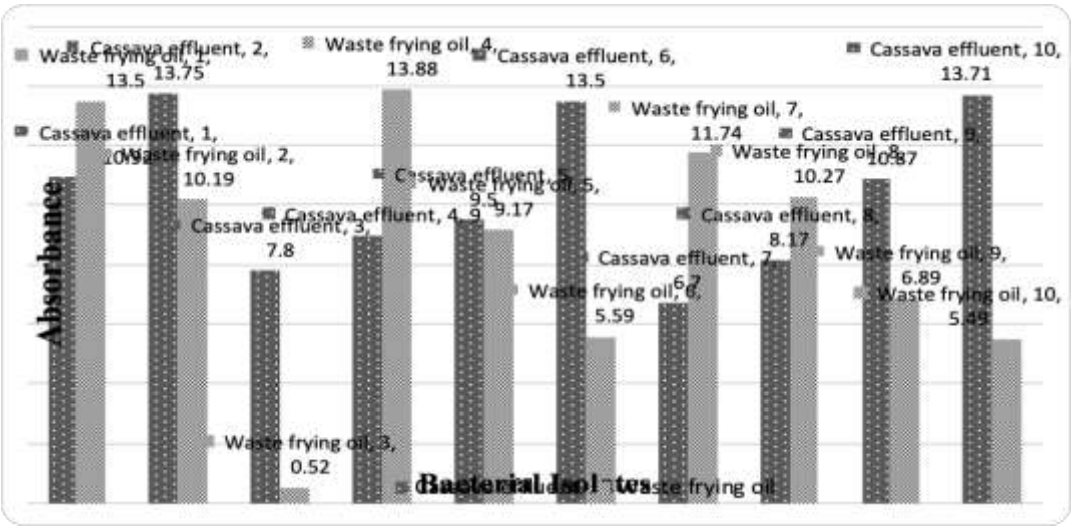

Fig. 3.3: Absorbance value taken after 72 hours from isolates grown in nitrogen limiting minimal salt medium in the presence of cassava effluent and waste frying oil as carbon source respectively

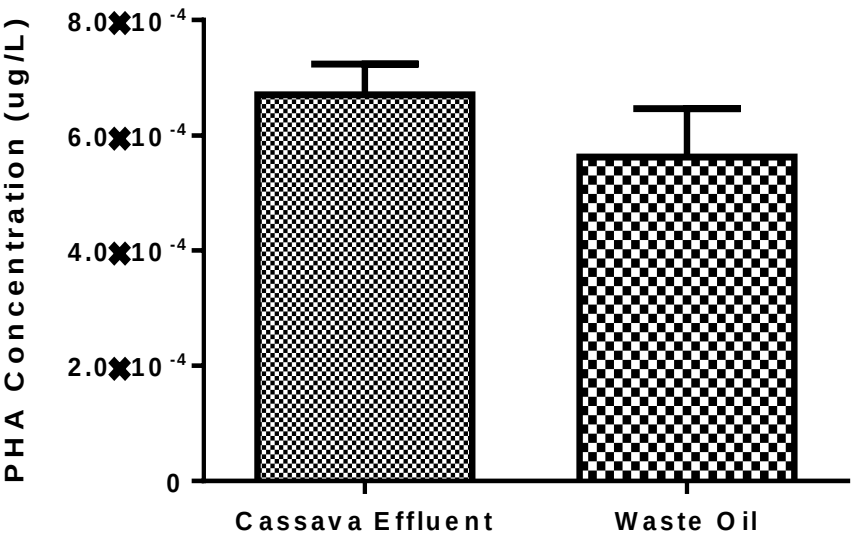

Fig 3.4: Cumulative concentration of PHA accumulated when cassava effluent and waste frying oil were used respectively as carbon source in a nitrogen-limiting medium

Data Analysis

The student t-test was used to determine the significant difference of concentrations obtained from both carbon sources. A P-value below 0.05 was considered significant. The t-test

conducted on the concentration of PHA accumulated, proved that there is no significant difference ($P<0.05$) between the concentrations of PHA obtained. Hence, either carbon source can be used as one does not render an advantage over the other [20]. Fatty acid analysis conducted by [21] proved that the residual nutrients from foods present in the waste frying oil contribute to increased PHA production.

Characterisation of PHA producing isolates

From the PHA accumulation evaluation, two isolates that had the highest PHA accumulation were selected each from a utilised carbon source. The selected isolates were further characterised using biochemical tests and by microscopy. The table below shows the cultural and biochemical features of the isolates capable of yielding high amounts of PHA while utilising cassava effluent/ waste frying oil as excess carbon source. The microscopy results shown in table 3.1 shows that the isolates are Gram's negative short rods. Their ability to hydrolyze starch indicates the presence of the enzyme amylase hence their ability to utilize cassava effluent as a carbon source. Obtained sequences were trimmed and submitted to the Genbank database under the following accession numbers MK989593, MK989594, MK989595 and MK989596. The DNA sequence of the four isolates were aligned with the 16S rRNA gene of similar genes in the NCBI database and were closely related to the Alcaligenes genus as adjudged by the phylogenetic trees in Figures 4.5 to 4.8. Sequence analysis showed that isolates Pairwise identity ranged from 96.1% to 100% for all isolates when compared with previously submitted sequences in the Genbank database. This confirms the PHA accumulation studies done on Alcaligenes spp. such as the study conducted by [22].

Table 3.1: Result showing the microscopic and biochemical characteristics of the selected bacterial isolates

CHARACTERISTICS	A1	A2	A4	A6
Gram's Reaction	-	-	-	-
Shape	Short rods	Short rods	Short rods	Short rods
Motility	Motile	Non-motile	Motile	Motile
Acid Fast Stain	-	-	-	-
Spore Stain	+	-	+	-
Citrate	+	+	+	+
	+	+	+	+
Catalase				
	-	-	-	-
Indole				
	-	-	-	-
MR	+	-	+	+
VP				
Starch Hydrolysis	+	+	+	+
Urease	-	+	-	+

	+	-	+	+
Oxidase				
	+	+	+	+
	+	-	+	-
Maltose				
Gas Production				
	+	+	+	+
Lactose	+	+	+	-
Gas Production				
	+	-	+	+
Sucrose	+	-	-	+
Gas Production				
	+	+	+	+
Growth at pH 6.0				
	+	+	+	+
Growth at 35˚C				
Growth in 5% NaCl	+	+	+	+

KEY: + indicates a positive Reaction
- indicates a negative Reaction

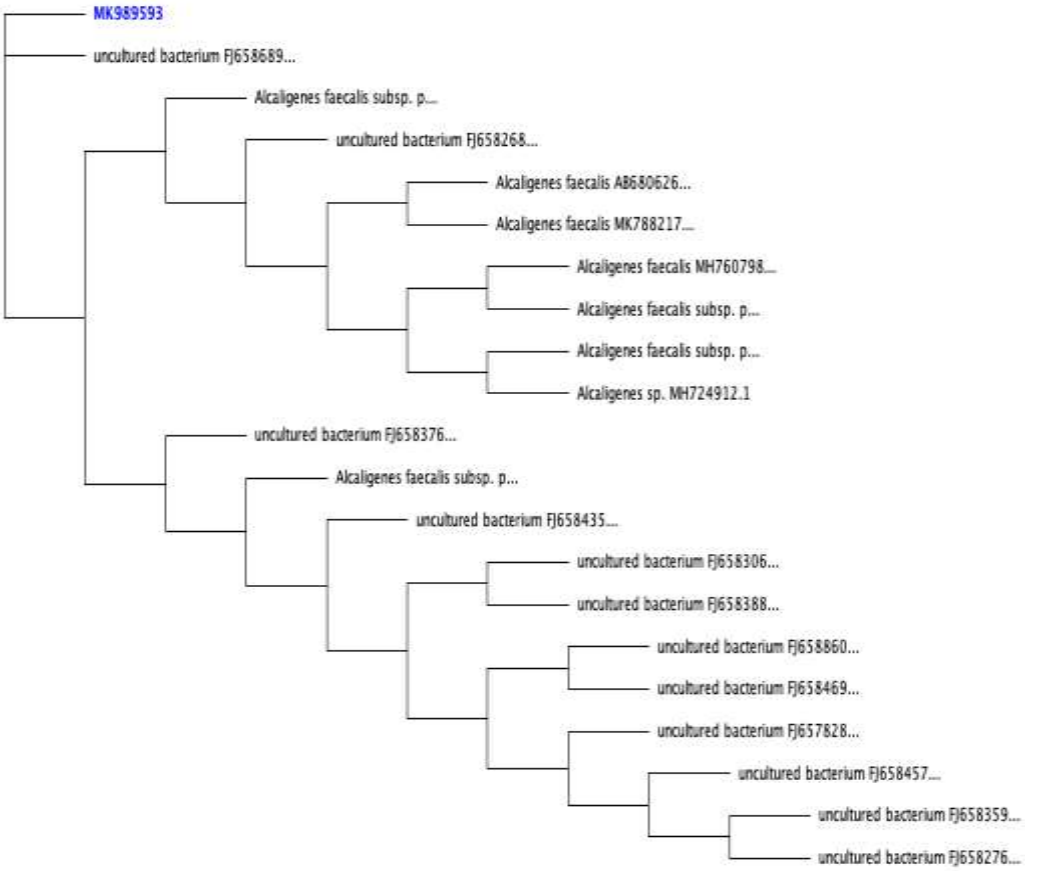

Fig 3.5: Phylogenetic tree of newly identified organism A1 with accession number MK989593 (source: Genious prime software). The DNA sequence of isolate A1 was aligned with the 16S rRNA gene of similar genes in the NCBI database and were closely related to the *Alcaligenesfaecalis* as well as other strains of *Alcaligenes faecalis* and various strains of uncultured bacterium. The genomic pairwise identity ranged from 96.1% to 100% when compared with previously submitted sequences in the Genbank database.

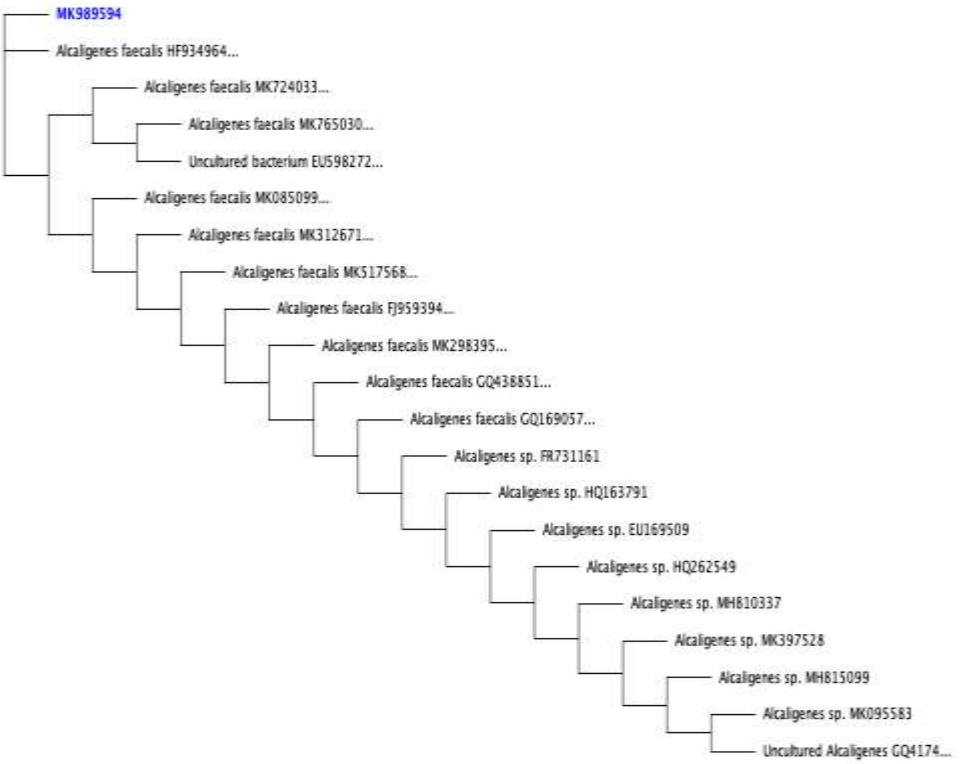

Fig 3.6: Phylogenetic tree of newly identified organism A2 with accession number MK989594 (source: Genious prime software). The DNA sequence of isolate A2 was aligned with the 16S rRNA gene of similar genes in the NCBI database and was found to be closely related to the *Alcaligenesfaecalis*, other species of *Alcaligenes* and various strains of uncultured bacterium. The genomic pairwise identity ranged from 96.1% to 100% when compared with previously submitted sequences in the Genbank database.

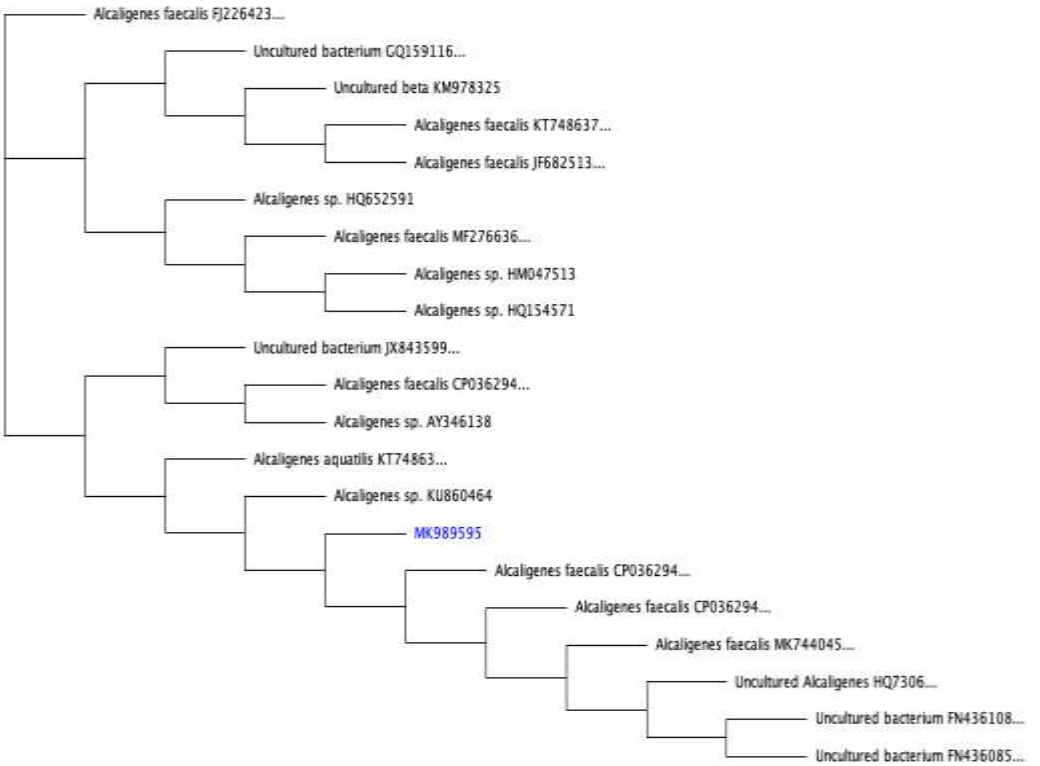

Fig 3.7: Phylogenetic tree of newly identified organism A4 with accession number MK989595 (source: Genious prime software). The DNA sequence of isolate A4 was aligned with the 16S rRNA gene of similar genes in the NCBI database and was found to be closely related to the *Alcaligenesfaecalis*, *Alcaligenesaquatilis* as well as other species of *Alcaligenes*and various strains of uncultured bacterium. The genomic pairwise identity ranged from 96.1% to 100% when compared with previously submitted sequences in the Genbank database.

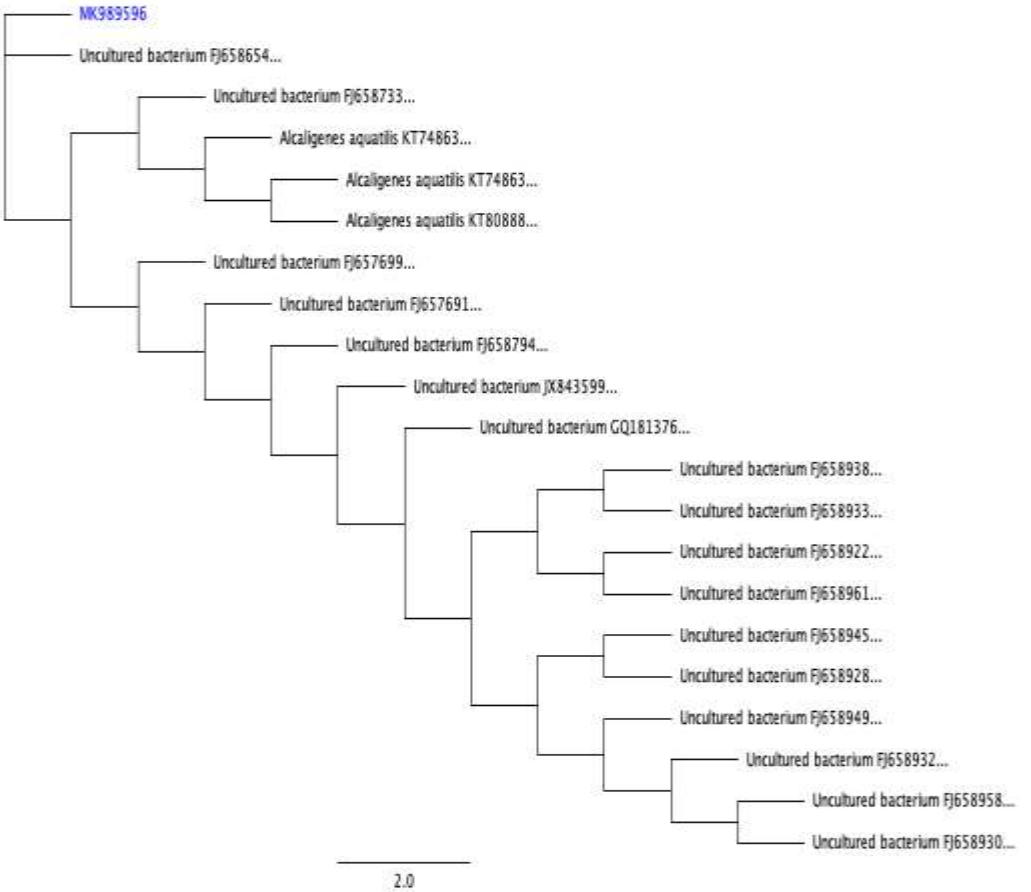

Fig 3.8: Phylogenetic tree of newly identified organism A6 with accession number MK989596 (source: Genious prime software). The DNA sequence of isolate A6 was aligned with the 16S rRNA gene of similar genes in the NCBI database and was found to be closely related to the Alcaligenesaquatilis and various strains of uncultured bacterium The genomic pairwise identity ranged from 96.1% to 100% when compared with previously submitted sequences in the Genbank database.

Polymer analysis using GCMS

The GC/MS was used to confirm the synthesis of PHA as proven by past studies [19, 23]. A study by [24] revealed the presence of phthalate produced from Bacillus spp, which is a type of plastic. Similarly, this present study revealed from the NIST-14 library of the GC/MS showed the presence of the polyhydroxyalkanoate called Methyl 2-hydroxy-heptadecanoate (Fig 3.9). It also revealed the presence of a type of plastic (phthalate) called isophthalic acid, di(6-ethyloct-3-yl) ester (Fig 3.10) and Bis(2-ethylhexyl) phthalate (Fig 3.11).

GC/MS Data File: Sample 1.D

Pk#	RT	Area%	Library/ID.	Ref#.	Cas#	Qual
94	21.372	1.60	C:\Database\NIST14.L			
			1-Docosene	167462	001599-67-3	93
			Heptacosyl acetate	253355	1000351-78-2.	83
			Methyl 2-hydroxy-heptadecanoate	159880	1000336-20-1	64
95	21.603	2.10	C:\Database\NIST14.L			
			Isophthalic acid, decyl phenyl est er	228549	1000344-36-3	35
			Terephthalic acid, decyl phenyl es ter	228553	1000324-06-8	27
			Terephthalic acid, 2-bromo-4-fluor ophenyl decyl ester.	262832	1000323-71-4	27
96	21.793	2.28	C:\Database\NIST14.L			
			3-Hydroxy-2,6,6-trimethyl-hept-4-e noic acid	52542	1000185-34-0.	46
			N-Carbethoxymethyliminomethylmalon ic acid methyl, ethyl ester	119715	1000223-03-2	44
			11-Methyl-octadecanoic acid, DMOX derivative	206508	1000336-95-2	44
97	22.122	0.94	C:\Database\NIST14.L			
			N-Carbethoxymethyliminomethylylmal onic acid dimethyl ester	106445	1000223-03-1	59
			2(1H)Naphthalenone, 3,5,6,7,8,8a-h exahydro-4,8a-dimethyl-6-(1-methyl ethenyl)-	81713	1000188-66-5	59
			1,1,3,5-Cyclohexanetetracarboxylic acid, 4-oxo-, tetramethyl ester	187606	051334-56-6	55
98	22.336	0.89	C:\Database\NIST14.L			
			N-Carbethoxymethyliminomethylylmal onic acid dimethyl ester	106445	1000223-03-1	76
			3,5-Dichloro-2',6'-difluorobipheny l-4-yl)methylamine	146702	1000306-72-7	55
			Butanedioic acid, 2,3-bis(8-nonen- 1-yl)-, dimethyl ester	235508	1000141-98-7	45

FIG 3.9: GC/MS NIST-14 library indicating the presence of Methyl 2-hydroxy-heptadecanoate

GC/MS DataFile: Sample 1.D

Pk#	RT	Area%	Library/ID.	Ref#.	Cas#	Qual
92	21.452	0.49	C:\Database\NIST14.L			
			Isophthalic acid, di(6-ethyloct-3-yl) ester	255782	1000344-68-0	50
			Isophthalic acid, decyl 3,5-dichlorophenyl ester	256586	1000356-58-9	50
			Isophthalic acid, 2-chloro-5-methylphenyl decyl ester	250799	1000356-57-2	50
93	21.551	0.05	C:\Database\NIST14.L			
			2,4,7,14-Tetramethyl-4-vinyl-tricyclo[5.4.3.0(1,8)]tetradecan-6-ol.	150240	1000193-31-2	89
			N'-(5,7-Dibromo-2-oxoindolin-3-ylidene)-2-(2-isopropyl-5-methylphenoxy)acethydrazide	267225	327033-93-2	89
			Phthalic acid, 4-trifluoromethylbenzyl ethyl ester	206891	1000371-04-1	76
94	21.689	0.64	C:\Database\NIST14.L			
			N'-(5,7-Dibromo-2-oxoindolin-3-ylidene)-2-(2-isopropyl-5-methylphenoxy)acethydrazide	267225	327033-93-2	86
			2-t-Butyl-6-[2-hydroxy-2-(2,4,6-trimethylphenyl)ethyl]-[1,3]dioxin-4-one	177033	1000192-88-0	64
			Phthalic acid, decyl 3-iodobenzyl ester	268733	1000378-07-4	64
95	22.024	0.51	C:\Database\NIST14.L			
			Cyclopentanecarboxamide, 3-ethenyl-2-(3-pentenylidene)-N-phenyl-, [1.alpha.,2Z(E),3.alpha.]-	141080	136091-23-1	56
			Furosemide tri-methyl derivative	221810	1000137-05-3	45
			1,2-Bis[4-quinolyl]ethene N-oxide	157964	1000211-32-3	44
96	22.163	0.48	C:\Database\NIST14.L			
			Cyclopentanecarboxamide, 3-ethenyl-2-(3-pentenylidene)-N-phenyl-, [1.alpha.,2Z(E),3.alpha.]-	141080	136091-23-1	90
			Thiocarbamic acid, N,N-dimethyl, S-1,3-diphenyl-2-butenyl ester	170048	1000192-89-2	64
			2,2-Dimethylpropanoic acid, 2,6-dimethylnon-1-en-3-yn-5-yl ester	111719	1000299-33-6	64

Fig 3.10: GC/MS NIST-14 library indicating the presence of isophthalic acid, di(6-ethyloct-3-yl) ester

5/13/2019 GC/MS DataFile: Sample 6.D

```
79  19.500  0.12 C:\Database\NIST14.L
              Nonadecane                          128835 000629-92-5 95
              Hexacosane                          217890 000630-01-3 94
              Heptadecane, 9-hexyl-               182660 055124-79-3 91

80  19.853  0.04 C:\Database\NIST14.L
              Bis(2-ethylhexyl) phthalate         233372 000117-81-7 68
              Diisooctyl phthalate                233366 000131-20-4 64
              Phthalic acid, di(2-propylpentyl)   233419 1000377-93-5 58
              ester

81  20.141  0.15 C:\Database\NIST14.L
              Eicosane                            142238 000112-95-8 98
              Nonadecane                          128835 000629-92-5 95
              Hexacosane                          217890 000630-01-3 94

82  20.592  0.01 C:\Database\NIST14.L
              Octacosane                          235614 000630-02-4 90
              Friedelan-3-one                     249550 000559-74-0 59
              1-Hexacosene                        216562 018835-33-1 59

83  20.759  0.11 C:\Database\NIST14.L
              Eicosane                            142238 000112-95-8 98
              Nonadecane                          128835 000629-92-5 95
              Heptadecane                         102600 000629-78-7 94

84  20.852  0.01 C:\Database\NIST14.L
              Androst-5,15-dien-3ol acetate       173513 1000251-88-0 38
              Pregna-5,16-dien-20-one, 3-hydroxy  173537 001162-53-4 38
              -, (3.beta.)-
              Benzoic acid, 4-(1,3-dioxolan-2-yl   72031 142651-24-9 35
              )-, methyl ester

85  21.135  0.02 C:\Database\NIST14.L
              17-Pentatriacontene                 265112 006971-40-0 90
              Octacosane                          235614 000630-02-4 59
              Eicosane                            142238 000112-95-8 58

86  21.354  0.13 C:\Database\NIST14.L
              Eicosane                            142238 000112-95-8 98
              Octacosane                          235615 000630-02-4 98
              Heptadecane, 9-octyl-               207503 007225-64-1 95

87  21.556  0.03 C:\Database\NIST14.L
              2,4,4-Trimethyl-3-hydroxymethyl-5a   85797 1000144-10-5 40
              -(3-methyl-but-2-enyl)-cyclohexene
              trans-Sesquisabinene hydrate         85739 145512-84-1 38
              Cyclopropanecarboxylic acid, hydra   72387 1000264-07-5 38
              zide, N2-cyclooctylideno-
```

Fig 3.11: GC/MS NIST-14 library indicating the presence of Bis(2-ethylhexyl) phthalate

Conclusion

From this study, organisms isolated from sites with high organic content, showed ability for PHA production on pilot scale. Isolates A1, A2, A4 and A6 were identified as *Alcaligenes* spp. and were the high PHA yielders. Hence, this study also paves way for further studies on the newly characterized species and for commercialization of PHA using waste frying oil and cassava effluents as substrates. Understanding the biosynthetic pathways of these organisms to producing PHAs and further manipulating the pathways would be key to achieving low and competitive production cost, as well as product design of the desired polymer. Other cheap substrates should be explored using these already characterised PHA producing strains.

References

Harshvardhan, K. and Jha, B. (2013) Biodegradation of low-density polyethylene bymarine bacteria from pelagic waters, Arabian Sea, India. Mar. Pollut. Bull. 77, 100–106

Urtuvia, V., Villegas, P., González, M. and Seeger, M. (2014) Bacterial production ofthebiodegradable plastics polyhydroxyalkanoates. Int. J. Biol. Macromol. 70, 208-213.

Zhao, Y. B., Lv, X. D. and Ni, H. G. (2018) Solvent-based separation and recycling of waste plastics: A review. Chemosphere 209, 707-720

Alimba, C. G., and Faggio, C. (2019) Microplastics in the marine environment: current trends in environmental pollution and mechanisms of toxicological profile. Environ. Toxicol. Pharmacol. 68, 61-74

Tamara, S.G., (2015) Micro- and nano-plastics and human health. In: Bergmann, M., Gutow, L., Klages, M. (Eds.), Marine Anthropogenic Litter (pp. 343). Springer, Berlin.

Cole, M., Lindeque, P., Halsband, C. and Galloway, T.S. (2011) Microplastics as contaminants in the marine environment: a review. Mar. Pollut. Bull. 62, 2588-2597.

Jambeck, J. R., Geyer, R., Wilcox, C., Siegler, T. R., Perryman, M., Andrady, A., Narayan,R. and Law, K.L. (2015) Plastic waste inputs from land into the ocean. Science 347, 768-771.

Geyer, R., Jambeck, J. R. and Law, K. L. (2017) Production, use, and fate of all plastics ever made. Sci. Adv. 3, e1700782

Raza, Z. A., Abid, S. and Banat, I. M. (2018) Polyhydroxyalkanoates: Characteristics, production, recent developments and applications. Int. Biodeterior. Biodegradation 126, 45-56.

Nwinyi, O.C. and Owolabi, T.A. (2017) Scanning electron microscopy and Fourier transmission analysis of polyhydroxyalkanoates isolated from bacteria species from abattoir in Ota, Nigeria. J. King Saud Univ Sci

Kourmentza, C., Plácido, J., Venetsaneas, N., Burniol-Figols, A., Varrone, C., Gavala, H. N., and Reis, M. A. (2017) Recent advances and challenges towards sustainable polyhydroxyalkanoate (PHA) production. J. Bioeng. 4(2): 55.

Chakravarty, P., Mhaisalkar, V., and Chakrabarti, T. (2010) Study on

poly-hydroxyalkanoate (PHA) production in pilot scale continuous mode wastewater treatment system. Bioresour. Technol. 101(8): 2896-2899.

Odusanya, S. A., Nkwogu, J. V., Alu, N., Udo, G. E., Ajao, J. A., Osinkolu, G. A., and Uzomah, A. C. (2013) Preliminary studies on microbial degradation of plastics used in packaging potable water in Nigeria. Niger. Food J. 31(2): 63-72.

Bhuwal, A. K., Singh, G., Aggarwal, N. K., Goyal, V., and Yadav, A. (2013) Isolation and screening of polyhydroxyalkanoates producing bacteria from pulp, paper, and cardboard industry wastes. Int. J. Biomater. 2013, 1-10.

Law, J. H., and Slepecky, R. A. (1960) Assay of poly-β-hydroxybutyric acid. J. Bacteriol. 82(1): 33-36.

Nishiguchi, M. K., Doukakis, P., Egan, M., Kizirian, D., Phillips, A., Prendini, L., Rosenbaum, H.C., Torres, E., Wyner, Y., DeSalle, R. and Giribet, G. (2002) DNA isolation procedures. In Techniques in molecular systematics and evolution (pp. 249-287). Birkhäuser, Basel.

Kumar, S., Stecher, G., and Tamura, K. (2016) MEGA7: molecular evolutionary genetics analysis version 7.0 for bigger datasets. Mol. Biol. Evol. 33(7): 1870-1874.

Numata, K., Morisaki, K., Tomizawa, S., Ohtani, M., Demura, T., Miyazaki, M., Nogi, Y., Deguchi, S. and Doi, Y. (2013) Synthesis of poly-and oligo (hydroxyalkanoate) s by deep-sea bacteria, Colwellia spp., Moritella spp., and Shewanella spp. Polym. J. 45(10): 1094.

Tan, G. Y., Chen, C. L., Li, L., Ge, L., Wang, L., Razaad, I., and Wang, J. Y. (2014) Start a research on biopolymer polyhydroxyalkanoate (PHA): a review. Polymers 6(3): 706-754.

Tufail, S., Munir, S., and Jamil, N. (2017) Variation analysis of bacterial polyhydroxyalkanoates production using saturated and unsaturated hydrocarbons. Braz. J. Microbiol. 48(4): 629-636.

Verlinden, R. A., Hill, D. J., Kenward, M. A., Williams, C. D., Piotrowska-Seget, Z., and Radecka, I. K. (2011) Production of polyhydroxyalkanoates from waste frying oil by Cupriavidus necator. AMB express 1(1): 11.

Sayyed, R. Z., and Chincholkar, S. B. (2004. Production of poly β-hydroxybutyrate from Alcaligenes faecalis. Indian J. Microbiol. 44(1): 269-272

Chanasit, W., Hodgson, B., Sudesh, K., and Umsakul, K. (2016) Efficient production of polyhydroxyalkanoates (PHAs) from Pseudomonas mendocina PSU using a biodiesel liquid waste (BLW) as the sole carbon source. Biosci. Biotechnol. Biochem. 80(7): 1440-1450.

Ali, W. S., Zaki, N. H. and Obiad, S. Y. N. (2017) Production of bioplastic by bacteria isolated from local soil and organic wastes. Curr. Res. Microbiol. Biotechnol. 5, 1012-1017.

Covenant Journal of Physical & Life Sciences (CJPL) Vol. 7 No. 2, Dec. 2019
ISSN: ***p. 2354 – 3574 e. 2354 – 3485*** **DOI:**

An Open Access Journal Available Online

Electronics and Optical Properties of Nitrogen Doped Anatase for Solar Application

Olayinka A. S.[1,*],Nwankwo W.[2] & Idiodi J. O. A.[3]

[1]Department of Physics, Edo University Iyamho, Edo State, Nigeria.
[2]Department of Computer Science, Edo University Iyamho, Edo State, Nigeria.
[3]Department of Physics, University of Benin, Benin city, Nigeria.

[*]akinola.olayinka@edouniversity.edu.ng; solayinkaa@gmail.com

Received: xxxx xxxxxx, 2019 Accepted: xxxx xxxxxx,, 2019
Date of Publication: December, 2019

Abstract: One of the major problems in developing countries is dearth of sufficient energy, which in turn hampers sustainable development. Anatase is one of the prominent polymorph of Titanium dioxide (TiO_2) with great potential for solar application except for its wide band gap which limits its solar energy utilization to about 4%. It has fascinated much devotion from researchers owing to its extensive array of applications coupled with its availability and cost effectiveness. Doping has been presented as a means to narrow the band gap thereby enhancing its efficiency for solar application. Electronic and optical properties are presented here for pure and Nitrogen (N) doped anatase. The study is based on the density functional theory (DFT) using generalized gradient approximation (GGA) in addition to Coulomb Interaction (U) as implemented in quantum espresso code while the optical properties calculation was done with the Yambo code. With the inclusion of U parameter of 12.5eV, band gap of 3.1eV was obtained which compared favorably with experimental results. Doping concentration of 3.1% gave rise to band narrowing while Partial density of state (PDOS) shows that the band narrowing in anatase is due to the contribution from 2p state of the Nitrogen dopant. The optical properties calculated revealed that N-doped anatase has optical crests in the visible light range of electromagnetic spectrum which makes it a potential material for solar application with higher efficiency than pure anatase.
Keyword: Anatase, doping, solar, dielectric constant.

Introduction

Recently, South Africa commissioned her first solar powered airport which happened to be the first in Africa after the first was launched in Indian few years ago. The airport generates 750 kW every day against 400kW required to run it daily[1]. African especially Nigeria is favoured in term of daily solar radiation of up to 220 W/m^2 as against about 150 W/m^2 for USA and 100 W/m^2 for Europe [2], thereby making it a stanch source of energy that is also renewable. Solar radiation is freely available; however, the major setback is the high cost associated with solar panels, making it inaccessible to the majority of growing populace in dare need of power to foster and drive sustainable developments. Anatase is a Polymorph of titanium dioxide (TiO_2) and it is a wide band gap material. $TiO_2$is nontoxic and relatively inexpensive. It is physically and chemically stable [3-5].TiO_2 is useful as photo-catalyst in solar applications, electric gas sensor, white pigments, biomaterials, memory devices and optical coatings [6-9]. TiO_2 is one of the important semiconductor photo-catalysts. A semiconductor photo-catalyst is a wide band gap semiconductor that can increase the rate of certain chemical reactions when exposed to light without directly participating in the reactions. The chemical/photochemical stability of TiO_2 is very high in comparison with other metal oxide materials[10]. It can be easily prepared and analysed by several experimental techniques thereby making it a preferred system for experimentalists [6].

Anatase is an auspicious material for Thin-Film solar panels except for its wide band gap which restrict it to utilize only about 4% of the solar energy[11]. The efficiency of monocrystalline is between 15-20% and polycrystalline between 13-16%. Thin-film solar panel prototypes have efficiencies range of 7–13% while production modules have efficiency of about 9% subject to manufacturing techniques. Future module efficiencies are anticipated to range between 10% and 16% [12]. Interest in thin-film solar panels was driven by the relevant advantages it offers like simple mass-production technique thereby dropping the price of solar panels drastically, it can be made flexible giving way to new potential applications. Temperature variation has less impact on its performance and it can be used where there is restriction in space.

In order to improve anatase efficiency for solar application, band gap narrowing has been suggested as a way for the material to absorb major part of the solar spectrum [11].Doping has been reported as a potential means of band narrowing for TiO_2[13]. Doping is the addition of impurities to in order to produce or modify the properties of a material. Doping anatase with Nitrogen (N) atom had been reported to improve optical absorption in the visible light region [14] due to band narrowing introduced by the dopant. However there is controversy on the source of the phenomenon responsible for band narrowing; it has been reported that band narrowing of anatase was due to mixing of the valence band with Nitrogen 2p states [15]; experimentalists reported that it was due to localized Nitrogen 2p states[14, 16] while other theoretical studies also concluded it was due to localized gap Nitrogen 2p states above the Valence band Maximum (VBM) because mixing of Nitrogen 2p and Oxygen 2p was considered too weak to yield substantial band narrowing[17, 18].

Optical properties of material refer to the response of such materials when exposed to electromagnetic radiation. Optical properties of materials are crucial and over the years it has been extensively investigated for several materials with promising applications. In order to investigate the optical properties of a material, it is necessary to study the complex dielectric function, ε(ω) which is defined as [19]

$$\varepsilon(\omega) = \varepsilon_1(\omega) + i\,\varepsilon_2(\omega) \quad (1)$$

where $\varepsilon_1(\omega)$ is the real part and $\varepsilon_2(\omega)$ is the imaginary part of dielectric function, which is mainly related to the electronic structure of a compound. Other optical constants, such as the refractive index n (ω), extinction coefficient k(ω), optical reflectivity R(ω), absorption coefficient α(ω), energy-loss spectrum L(ω), and complex conductivity function σ(ω), can be gained from the complex dielectric function ε(ω). The imaginary part of dielectric function describes electronic absorption of materials while the real part relates to the electronic polarizability of materials. The real part of the complex dielectric function $\varepsilon_1(\omega)$ can also be evaluated from the imaginary part $\varepsilon_2(\omega)$ through the famous Kramer's Kronig relationship [19].The imaginary part of the dielectric constant $\varepsilon_2(\omega)$ can be described as [20, 21]

$$\varepsilon_2(\hbar\omega) = \frac{2e^2\pi}{\Omega\varepsilon_0}\sum_{c,v}\sum_{k}\left|\left\langle\psi_k^c\left|\hat{u}.r\right|\psi_k^v\right\rangle\right|^2\delta\left(E_k^c - E_k^v - \hbar\omega\right) \quad (2)$$

where **Ω** is the volume of the elementary cell, vector u represents the polarization direction of the electric field of the incident photon, v represents the valence band while c represents the conduction band, k represents the reciprocal lattice vector, and ω represents the frequency of the incident photon while ħ represents the normalised Planck constant. $\left\langle\psi_k^c\left|\hat{u}.r\right|\psi_k^v\right\rangle$ represents the matrix elements that determine the probabilities of excitations of electrons occurring from the energy levels in the valence band (E_k^v) to the energy levels in the conduction band (E_k^c) i.e. inter-band transitions.

Equation 1 shows the relationship between the dielectric function, ε(ω) and imaginary part of dielectric function $\varepsilon_2(\omega)$ while equation 2 shows the relationship that exists between the imaginary part of dielectric function $\varepsilon_2(\omega)$ and electronic band structure. Optical transition peaks correspond to optical transitions between two states while the intensity of peaks is proportional to density of states.

The valence electronic configurations of the pseudopotentials are $2s^22p^4$ for oxygen, $2s^22p^3$ for nitrogen and $3s^23p^63d^24s^2$ for titanium because only the outer shell electrons are considered. Inner shell electrons are often localized around its ion and do not contribute to covalent bonds. So, instead of a physical potential for the nucleus and the inner electrons, a pseudopotential is used that simulates the effects of a nucleus potential that is screened by its inner electrons. The 2x2x1 supercell of pure anatase TiO_2 consists of 48 atoms (i.e. 16 Titanium atoms and 32 Oxygen atoms). For the N doped anatase one out of the 32 oxygen atoms was replaced with one Nitrogen atom which

corresponds to 3.1% impurity level of doping.

Computational Methodology

Anatase is a tetragonal structure with space group number 141 (space group D_4h^19-I4_1/amd with Patterson symmetry I4/mmm) containing four titanium (cations) and eight oxygen (anions) atoms [22]. The titanium atoms are located at the Wyckoff positions 8(c) while the oxygen atoms occupied the 16(f) Wyckoff positions as highlighted in table of Wyckoff position for space group 141 in Table 1 respectively, the internal parameter, x of 0.208 was used[23].

Table 1: The Wyckoff positions of the group 141 (I41/amd)[23]

Atom	Multiplicity	Wyckoff letter	Site symmetry	Coordinates
O	16	f	.2.	(x,0,0) (-x+1/2,0,1/2) (1/4,x+3/4,1/4) (1/4,-x+1/4,3/4) (-x,0,0) (x+1/2,0,1/2) (3/4,-x+1/4,3/4) (3/4,x+3/4,1/4)
Ti	8	c	.2/m.	(0,0,0) (1/2,0,1/2) (1/4,3/4,1/4) (1/4,1/4,3/4)

The atomic positions for bulk anatase was generated based on the Wyckoff positions 8(c) for Ti atoms and 16(f) for Oxygen highlighted in Table 1. The generated atomic positions for bulk anatase are:

Ti 0.000000000 0.000000000 0.000000000
Ti 0.500000000 0.000000000 0.500000000
Ti 0.250000000 0.750000000 0.250000000
Ti 0.250000000 0.250000000 0.750000000
O 0.208000000 0.000000000 0.000000000
O 0.292000000 0.000000000 0.500000000
O 0.250000000 0.958000000 0.250000000
O 0.250000000 0.042000000 0.750000000
O -0.208000000 0.000000000 0.000000000
O 0.458000000 0.000000000 0.500000000
O 0.750000000 0.042000000 0.750000000
O 0.750000000 0.958000000 0.250000000

The structures of anatase are shown in Fig. 1 for primitive unit cell, pure 2x2x1 supercell and N-doped 2x2x1 supercell with label A, B and C respectively. The Brillouin zone integration was done using the Monkhorst-Pack set of k-points[24]. Tetrahedron method was used for density of states (DOS) calculation with Blöchl corrections for precision [25]. The geometry of anatase TiO_2 bulk parameters was optimised using Broyden-Fletcher-Goldfarb-Shanno (BFGS) scheme [26]at different sets of k-points and energy cutoff to evaluate their effects on the bulk parameters. In order to dope(introduce a

moderate impurity to alter electronic and optical properties) anatase TiO_2 with Nitrogen (N), we created a 2x2x1 supercell from the bulk anatase as shown in fig 1(B), thereafter; one oxygen atom was substituted with a Nitrogen atom as shown in fig 1(C). The 2x2x1 N-doped anatase TiO_2 is made up of 16 Ti atoms, 31 oxygen atoms and 1 Nitrogen atom ($T_{16}O_{31}N_1$) which gives an impurity level of 3.1% concentration. Guoet al[27]stated that anatase TiO_2 doped with metal usually suffers from thermal instability and electronic states of cationic dopant may serve as carrier recombination centers leading to the photo-catalytic ability being decreased thus we decided to doped anatase with Nitrogen which is a non-metal.

To account for the strongly correlated interactions of the Ti d electrons (i.e. d–d Coulomb interaction in the titanium atoms), a moderate on-site Coulomb Repulsion U=12.5eV was applied to the calculation of electronic structures so as to obtain a more accurate electronic band gap comparable to experimental value of 3.20eV [28]. The choice of U was made after a series of calculations with different Coulomb interaction parameters, U.

The optical properties calculations for pure and doped anatase were performed within the Density Functional Theory (DFT) as implemented in quantum expresso code[29]to investigate their ground state properties. The ground state properties are then post-processed by Linear Response Theory according to the Bethe-Salpeter-Equation (BSE[30])as implemented in YAMBO code[31].

.

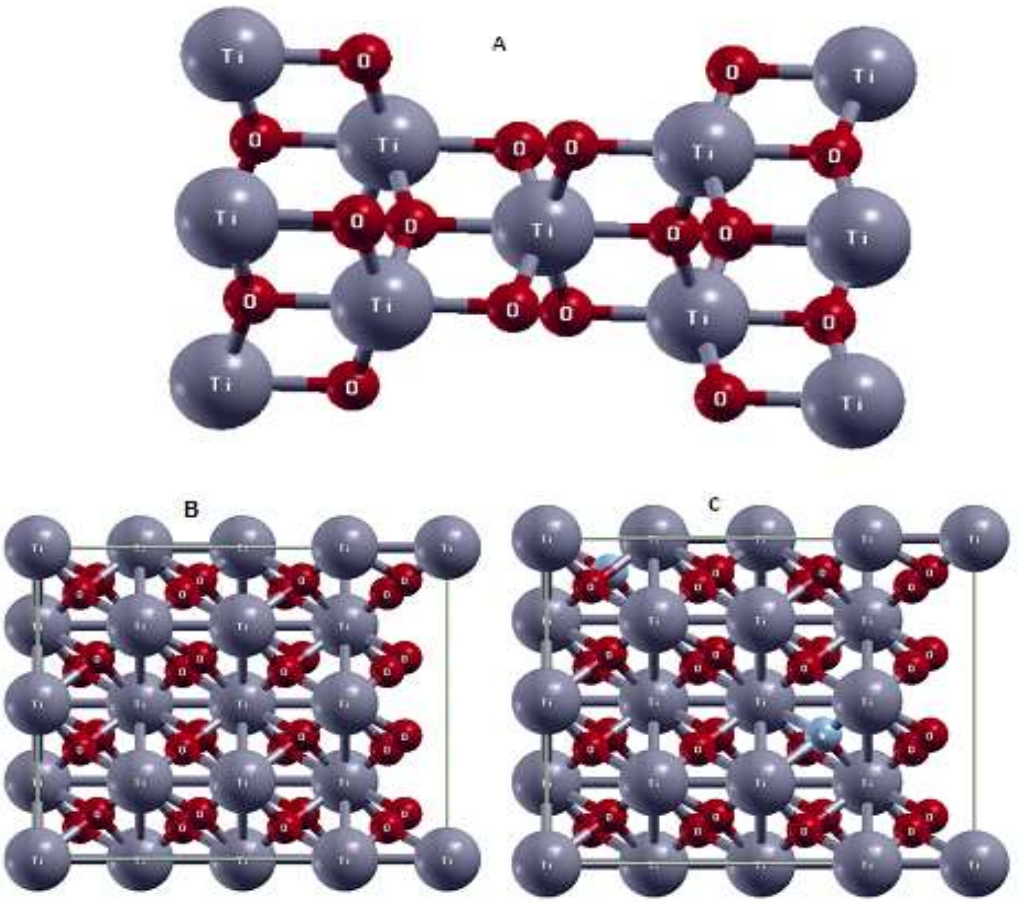

Fig. 1: (A) The tetragonal unit cell of Anatase Structure. (B) Pure Anatase 221 Supercell. (C) is 3.1% N-Doped Anatase 221 Supercell(Drawn using xcrysden[32])

Results and Discussion

Electronic Properties

The 2D-cut of the charge density map for Anatase TiO_2 and the electron density map for Anatase TiO2 along (100) plane are shown in figure 2.The band structure calculation for anatase followed the high symmetry points of the Brillouin Zone for Body Centred Tetragonal (BCT1) system as shown in figure 3(a) from where we adopted the high symmetry direction of Z – Γ – X – P – N – Γ shown in figure3(b). The calculated band structures for anatase TiO_2 within the local density approximation (LDA) with exchange correlation functional PZ (Perdew and Zunger) [33]and CP (Cole and Perdew) [34] gave indirect band gap of approximately 2.20eV (i.e. 2.21eV and 2.18eV respectively), obtained between X and P points for both functional. For the exchange correlation functional of Becke –Lee – Yang – Parr, BLYP [35,

36] and Perdew – Burke – Ernzerhof, PBE [37], indirect band gap of 2.36eV was obtained between X and P points. Results for band gaps (2.21eV, 2.18eV and 2.36eV) obtained for both LDA and GGA calculations compares favorably with available theoretical calculations results [38-40]as shown in Table 2. However, they are all considered to underestimate the band gap with respect to the experimental result of 3.2eV[28]. This underestimation of band gaps can be attributed the choice of exchange correlation functional as can be seen from the results where different functionals gave different electronic band gaps which is a general deficiency attributed to density functional theory (DFT). The accuracy of DFT calculation is directly related to the accuracy of the functional used.

Fig. 4 shows the Electronic Band Structure of pure Anatase along the high symmetry directions of the Brillouin zone within framework of the GGA + U approach. The calculation was done with Exchange-correlation functional of Becke-Lee-Yang-Parr, BLYP [35, 36]. The band gap of 3.10eV was obtained which compares better with experimental result of 3.20eV of Burdett et al.[28].

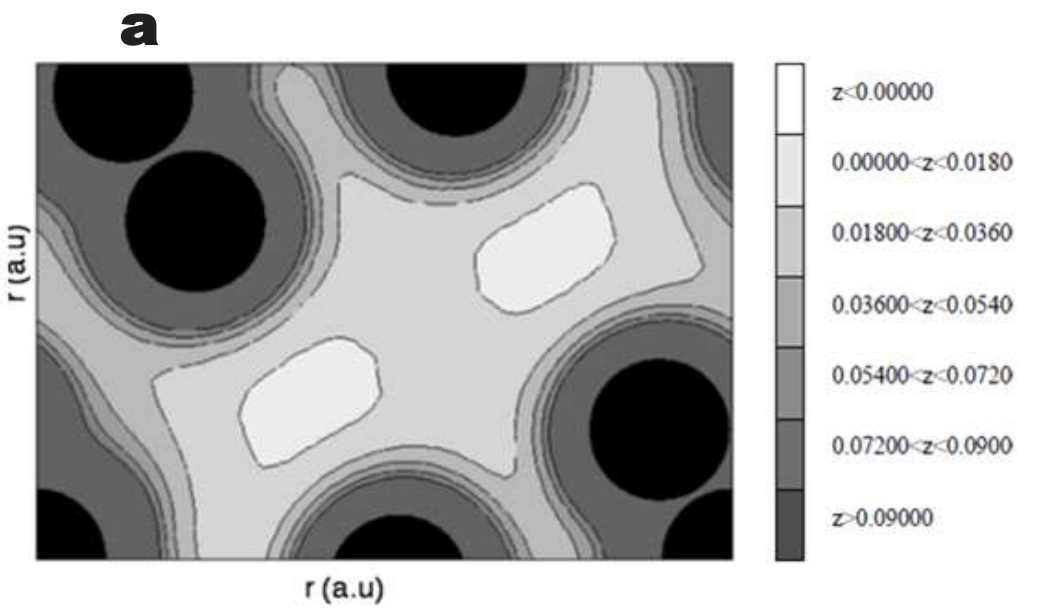

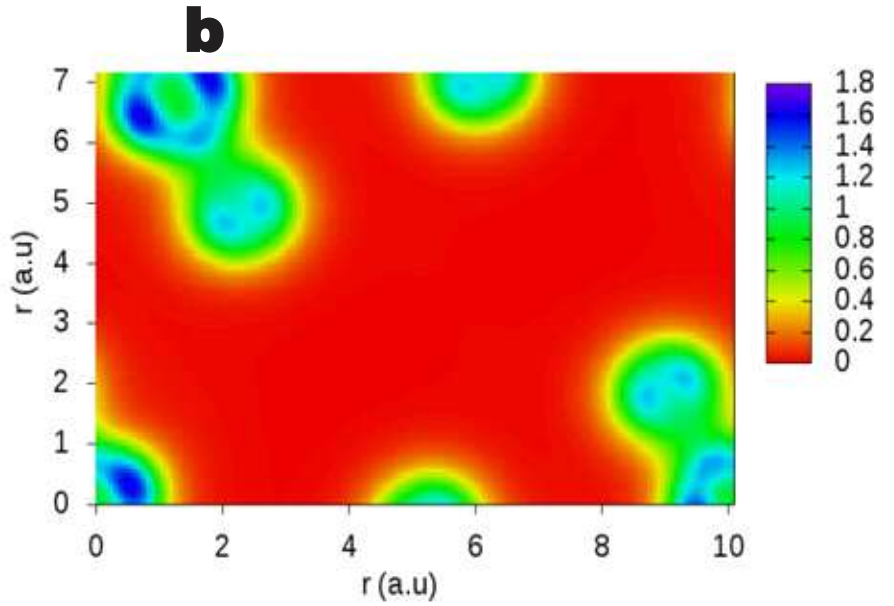

Fig. 2: (a) 2D Cut of the Charge Density of Anatase. (b) Electron Density Map for Anatase

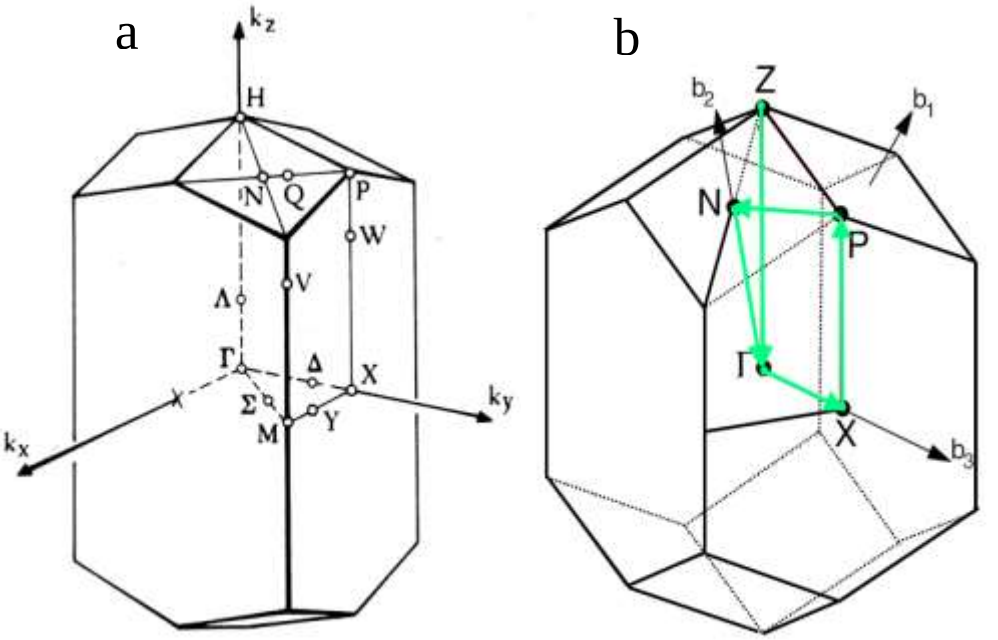

Fig. 3: (a) Brillouin Zone high symmetry points for Body Centred Tetragonal system (b) High Symmetry points direction for Anatase Band Structure Calculation (Points generated with xcrysden)

Table 2: Comparison ofour calculated band gap and lattice parameters for anatase TiO_2 with available theoretical and experimental results

BandGap E_g(eV)	Lattice Parameter		Potential	Code / Method	Reference
	a (Å)	c (Å)			
Theoretical Results					
2.18[I],2.21[I]	3.8182	9.6871	LDA-DFT	Quantum Espresso	This Work
2.36[I] 2.39[I] 3.10	3.7121 3.7751 3.7751	9.5802 9.5116 9.5116	GGA-DFT BLYP GGA-DFT PBE GGA-DFT+U(12.5eV) PBE		
2.15[I], 2.43 3.83[I], 4.29	3.81	9.64	GGA-DFT PBE GoWo	Quantum Espresso GoWo	[38]
2.34	3.801	9.778	PBE-GGA	CASTEP	[41]
2.679	-	-	mBJ FPAPW	WIEN2K	[42]
2.8[I]	3.832	9.599	GGA+U	VASP	[43]
2.11 2.295	3.829	9.702	GGA-DFT GGA+U	CASTEP	[44]
2.13	3.80	9.67	GGA-DFT PBE	CASTEP	[45]
2.3	-	-	LAPW	WIEN2K	[46]
2.811	3.7973	9.7851	GGA PW91	CASTEP	[47]
2.12	3.784	9.515	DFT	CASTEP	[48]
2.14[I] 2.89[I]	-	-	GGA-DFT GGA-DFT+U (6.6eV)	CASTEP	[49]
2.0	3.77	9.46	FP-LAPW	VASP	[50]
Experimental Results					
			Method		
3.20	3.785	9.502	Pulsed Neutron Diffraction		[28]
3.3	3.784	9.515	Absorption Photodesorption of Oxygen		[51]

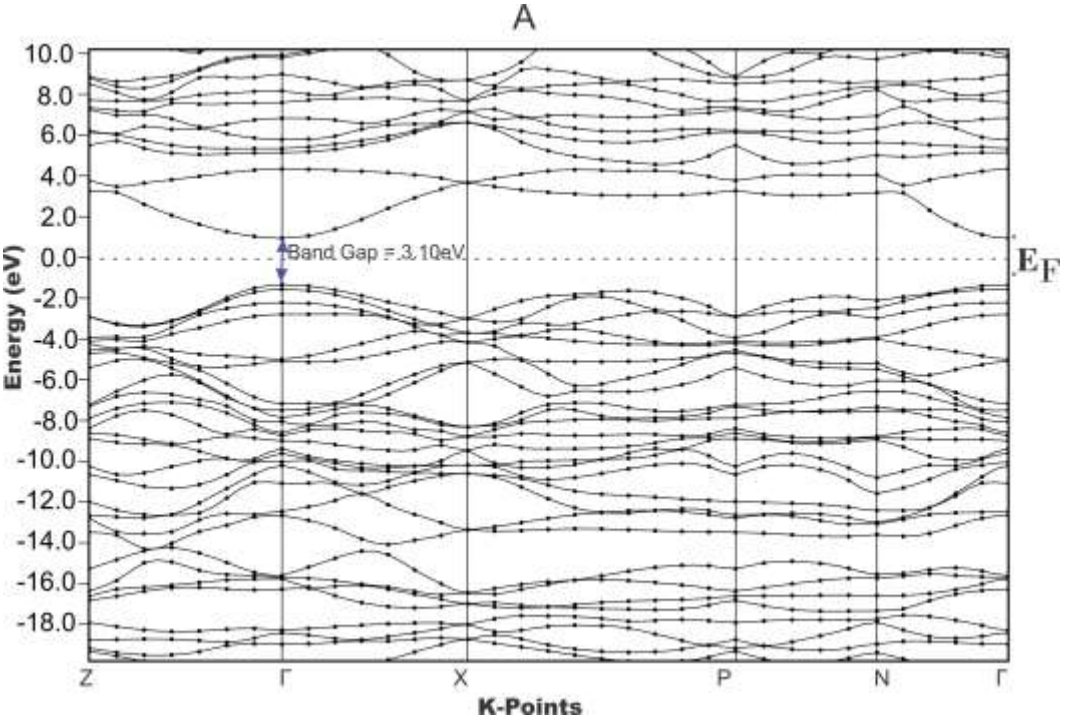
A
10.0
8.0
6.0
4.0
2.0
0.0
-2.0
-4.0
-6.0
-8.0
-10.0
-12.0
-14.0
-16.0
-18.0
Energy (eV)
Band Gap = 3.10eV
E_F
Z
Γ
X
P
N
Γ
K-Points

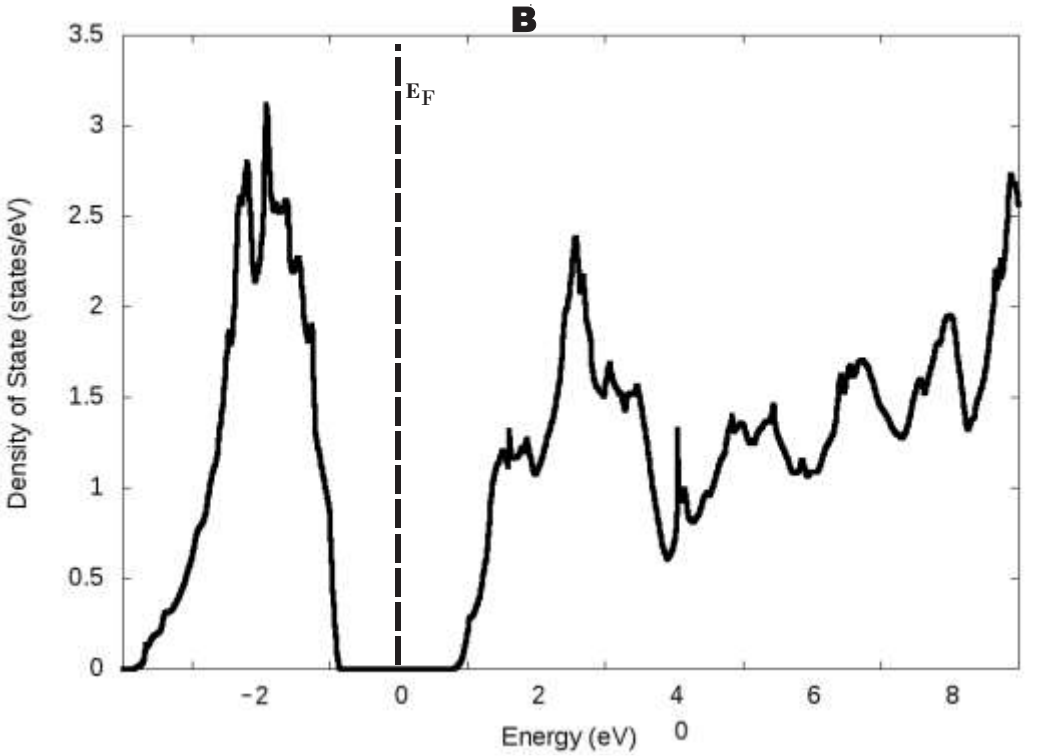

Fig. 4: (A) is the Band Structure of Pure Anatasefor GGA+U Calculation. (B)is DOS from A.

The Partial density of states (PDOS) for all states in anatase TiO_2 shows that the valence band maximum (VBM) of pure anatase TiO_2 predominantly consists of the O 2p states while the conduction band minimum (CBM) is predominantly of Ti d states, however, the hybridization between the Ti d and O 2p levels at the valence band can be observed.PDOS reveals the bands of electronic band structure with respect to their electronic states and contribution to the band gap. The lowest part of the valence bands are predominantly made up of O – 2(s) states with little mixture of the Ti – p and Ti – s states.

The band structure for the N-doped anatase is shown in Fig. 5 with a direct band gap of 1.47eV at Γ point. There was a shift in the Fermi level of the N-doped anatase band structure towards the conduction band, which may be due to charge balance between the dopant and the host lattice. This shift in the Fermi level thereby contribute to the reduction in the band gap as also reported by [45] for their Ag (Silver) doped anatase. PDOS shows that the valence bands consist mainly of the O 2p states within the energy range of -4.0eV and 0eV while conduction band is predominantly Ti 3d states within the energy range of 0eV and 6.0eV. The

extra band between VBM and CBM can be seen to come from the N 2p states as a result of the Nitrogen dopant. It can be inferred that nitrogen impurity atom (dopant) was able to modify the electronic structure of anatase.

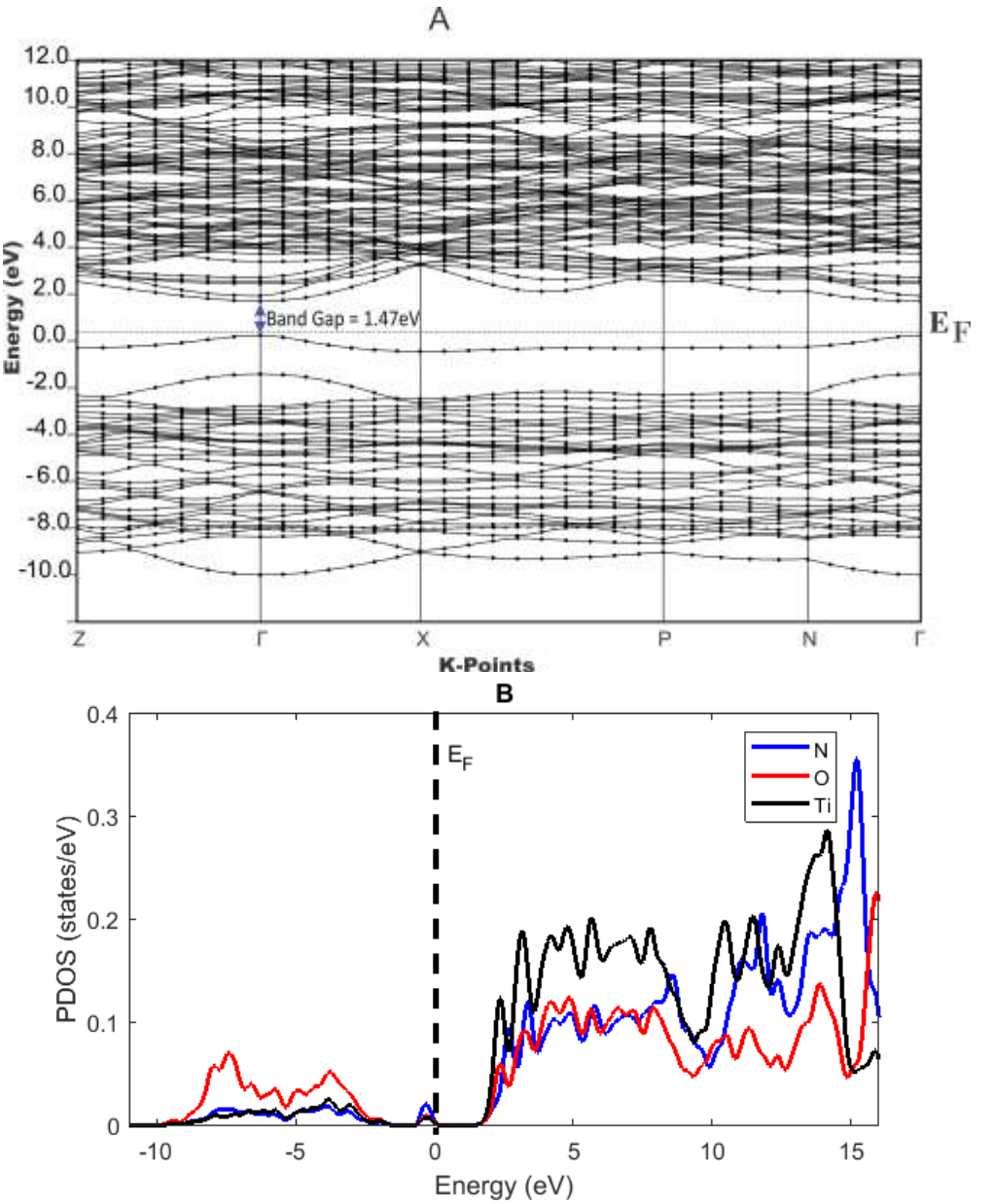

Fig. 5: A is Band Structure of 3.1% N-Doped Anatase ($Ti_{16}O_{31}N_1$). B is the Calculated PDOS for A.

Optical Properties

Figure 6 shows the comparison of the imaginary part of the frequency dependent dielectric spectrum for pure and N-doped anatase TiO_2. The comparison of the real part of the dielectric spectrum for pure and N-doped anatase TiO_2 indicate six different optical peaks for doped specie at D1 to D6 with respective energy values of 0.5eV, 0.7eV, 1.2eV, 1.8eV, 2.3eV and 3.5eV. The result obtained by [49]for N-doped anatase shows two peaks at about 1.8eV and 4.22eV. For the pure anatase with increase of energy response, 5.5eV optical transition can be observed, which indicate optical response of the imaginary part of the dielectric function for band gap. After doping with nitrogen, N the optical transition from band gap decreases to 3.5eV. This shift of the optical transition indicates that the band gap of the doped anatase was reduced as described in our result for the band structure and density of states (DOS). The highest peak transition was observed at 0.7eV in the low energy region which can lead to the shift of valence band to dopant states.

The intrinsic anatase shows the optical absorption peaks at the ultraviolet (UV) region of the electromagnetic spectrum while the N-doped anatase has optical absorption peaks in the visible light region. N-doped anatase shows a wider range of optical absorption peaks than N-doped rutile which may be due to presence of a more distinct band between the Valence Band Minimum (VBM) and Conduction Band Maximum (CBM). This band between the VBM and CBM comes from the contribution of N 2p states as seen earlier in the partial density of states (PDOS) for N-doped anatase. These widely distributed optical peaks may be able to increase the absorption of photons in the visible light region of the electromagnetic spectrum.

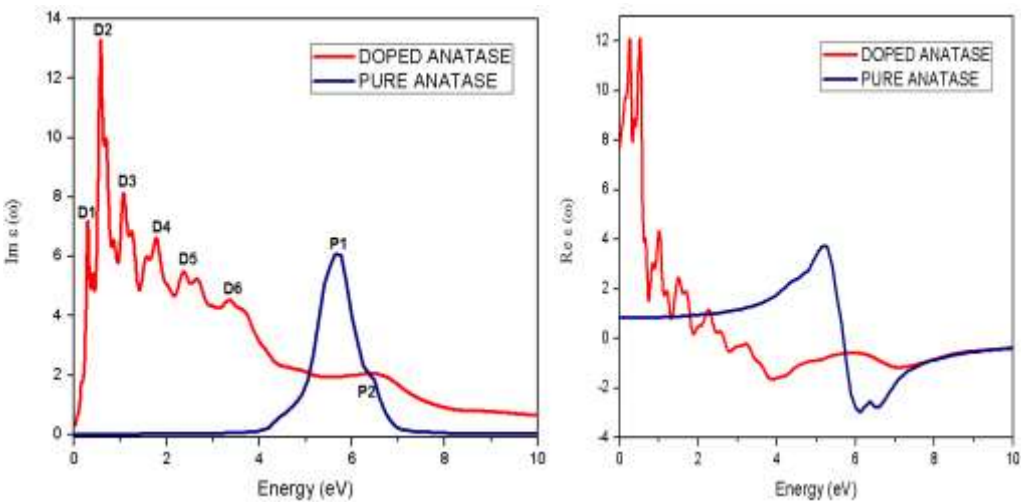

Fig. 6: Comparison of Imaginary part and real part of the frequency dependent dielectric function of Pure Anatase and 3.1% Concentration N-Doped Anatase respectively.

Conclusion

In this work, the electronic and optical properties of body centered tetragonal TiO_2 anatase (pure and doped) have been carried out within the density functional theory in the local density approximation (LDA) and the generalized gradient approximation (GGA)with the inclusion of Coulomb interaction parameter, U. The energy band gap, the density of states, partial density of states and frequency dependent dielectric functions were calculated. Pure anatase have their Fermi level located in the gap showing insulating properties. Doping with one Nitrogen atom resulted in the upward shift of Fermi level towards the conduction band thereby reducing the band gap. From the optical properties of N-doped anatase analysis, N-doped anatase may be a good base material for photovoltaic application because of the optical peaks exhibited in the visible light region of electromagnetic spectrum.

Acknowledgement

Olayinka A.S. wishes to thank ForschungszetrumJulich, Germany and ICTP (Ref: 23100000) for the respective supports in the course of this research.

References

respective supports

[1] Debut B. (2016) South Africa Basks in Continent's First Solar-Powered Airport. http://phys.org/news/2016-10-south-africa-basks-continent-solar-powered.html;

[2] Ajayi O.O., Ohijeagbon, O.D, Nwadialo, C.E. and Olasope, O. (2014). New Model to Estimate Daily Global Solar Radiation over Nigeria. Sus. Energy Tech. & Ass. 5, 28-36.

[3] Long R., English N.J. (2010). Electronic Properties of F/Zr Co-Doped Anatase Tio2 Photocatalysts from Gga+ U Calculations. Chem. Phy. Lett. 498, 338-44.

[4] O'regan B., Grätzel M. (1991). A Low-Cost, High-Efficiency Solar Cell Based on Dye-Sensitized Colloidal TiO_2 Films. Nature 353. 737.

[5] Devi L.G., Murthy B.N., Kumar S.G. (2009). Photocatalytic Activity of V^{5+}, Mo^{6+} and Th^{4+} Doped Polycrystalline TiO_2 for the Degradation of Chlorpyrifos under UV/Solar Light. J. of mol. catal A: Chem. 308, 174-81.

[6] Diebold U. (2003). The Surface Science of Titanium Dioxide. Surf. Sc. Reports 48, 53-229.

[7] Olayinka, A. S., Adetunji, B. I., Idiodi, J. O. A. and Aghemelon U. (2019). Ab initio study of electronic and optical properties of nitrogen-doped rutile TiO_2. Int. J. of Mod. Phy. B. 33(06), 1950036

[8] Diebold U. (2003). Structure and Properties of TiO_2 Surfaces: A Brief Review. App. Phy. A 76, 681-7.

[9] Gong X.-Q., Selloni A., Vittadini A. (2006). Density Functional Theory Study of Formic Acid Adsorption on Anatase TiO_2 (001): Geometries, Energetics, and Effects of Coverage, Hydration, and Reconstruction. The J. of Phy Chem. B 110, 2804-11.

[10] De Lasa H., Serrano.B. and Salaices M., (2005) Photocatalytic Reaction Engineering. Springer Science,

Business Media Inc., Spring Street, New York, NY10013.

[11] Han X. and Shao G. (2011). Electronic Properties of Rutile TiO_2 with Nonmetal Dopants from First Principles. The J. of Phy. Chem. C **115**, 8274-82.

[12] Maehlum M.A. (2015). Which Solar Panel Type Is Best? Mono- Vs. Polycrystalline Vs. Thin Film. http://www.energyinformative.org/best-solar-panel-monocrystalline-polycrystalline-thin-film/ 2015.

[13] Mi L., Xu P., Shen H., Wang P. N., and Shen W. (2007). First-Principles Calculation of N: H Codoping Effect on Energy Gap Narrowing of TiO_2. App. Phy. Lett. **90**, 171909.

[14] Irie H., Watanabe Y., Hashimoto K. (2003). Nitrogen-Concentration Dependence on Photocatalytic Activity of Tio2-X N X Powders. The J. of Phy. Chem. B **107**, 5483-6.

[15] Asahi R., Morikawa T., Ohwaki T., Aoki K., Taga Y. (2001). Visible-Light Photocatalysis in Nitrogen-Doped Titanium Oxides. Science **293**, 269-71.

[16] Lindgren T., Mwabora J., Avendano E., Jonsson J., Hoel A., Granqvist C. G and Lindquist S. E. (2003). Photoelectrochemical and Optical Properties of Nitrogen Doped Titanium Dioxide Films Prepared by Reactive DC Magnetron Sputtering. J. Phys Chem B.**107(24)**, 5709-5716.

[17] Lee J.-Y., Park J., and Cho J.-H. (2005). Electronic Properties of N-and C-Doped TiO_2. App. Phy. Lett. **87**, 011904.

[18] Long M., Cai W., Wang Z., and Liu G. (2006). Correlation of Electronic Structures and Crystal Structures with Photocatalytic Properties of Undoped, N-Doped and I-Doped TiO_2. Chem. Phy. Lett. **420**, 71-6.

[19] Ambrosch-Draxl C., and Sofo J.O. (2006). Linear Optical Properties of Solids within the Full-Potential Linearized Augmented Planewave Method. Comp. Phy. Comm. **175**, 1-14.

[20] Ibach H., and Lüth H. (2009) Dielectric Properties of Materials. Solid-State Physics: Springer;. p. 371-418.

[21] Wooten F. (1972). Optical Properties of Solids, Academic, New York.

[22] Tilley R. (2006). Crystal and Crystal Structures: John Wiley & Sons Ltd, West Sussex, England.;

[23] Aroyo M.I., Perez-Mato J.M., Capillas C., Kroumova E., Ivantchev S., Madariaga G., Kirov A. and Wondratschek H. . (2006). Bilbao Crystallographic Server I: Databases and Crystallographic Computing Programs. Z Krist **221**, 1527.

[24] Monkhorst H.J., Pack J.D. (1976). Special Points for Brillouin-Zone Integrations. Phy. Rev. B **13**, 5188.

[25] Blöchl P.E., and Jepsen O., Andersen O.K. (1994).

Improved Tetrahedron Method for Brillouin-Zone Integrations. Phy. Rev. B **49**, 16223.

[26] Fischer T.H., and Almlof J. (1992). General Methods for Geometry and Wave Function Optimization. The J.of Phy. Chem. **96**, 9768-74.

[27] Guo W., Wu L., Chen Z., Boschloo G., Hagfeldt A., and Ma T. (2011). Highly Efficient Dye-Sensitized Solar Cells Based on Nitrogen-Doped Titania with Excellent Stability. J. of Photochem.and Photobio. A: Chem. **219**, 180-7.

[28] Burdett J.K., Hughbanks T., Miller G.J., Richardson Jr J.W., and Smith J.V. (1987). Structural-Electronic Relationships in Inorganic Solids: Powder Neutron Diffraction Studies of the Rutile and Anatase Polymorphs of Titanium Dioxide at 15 and 295 K. J. of the American Chem. Soc. **109**, 3639-46.

[29] Giannozzi P., Baroni S., Bonini N., Calandra M., Car, R., Cavazzoni C., Ceresoli D., Chiarotti G. L., Cococcioni M., Dabo I., Dal Corso A., Fabris S., Fratesi, G., de Gironcoli S., Gebauer R.., Gerstmann U., Gougoussis C., Kokalj A., Lazzeri M., Martin-Samos L., Marzari N., Mauri F., Mazzarello R., Paolini S., Pasquarello A., Paulatto L., Sbraccia C., Scandolo S., Sclauzero G., Seitsonen A. P., Smogunov A., Umari P. and Wentzcovitch R. M. (2009). QUANTUM ESPRESSO: a modular and open-source software project for quantum simulations of materials. J. Phys.: Condens. Matter **21**, 395

[30] Salpeter E.E., and Bethe H.A. (1951). A Relativistic Equation for Bound-State Problems. Phy.Rev. **84**, 1232.

[31] Marini A., Hogan C., Grüning M., and Varsano D. (2009). Yambo: An Ab Initio Tool for Excited State Calculations. Comp. Phy. Comm. **180**, 1392-403.

[32] Kokalj A. (2003). Computer Graphics and Graphical User Interfaces as Tools in Simulations of Matter at the Atomic Scale. Comp. Mat. Sc. **28**, 155-68.

[33] Perdew J.P., and Zunger A. (1981). Self-Interaction Correction to Density-Functional Approximations for Many-Electron Systems. Phy. Rev. B **23**, 5048.

[34] Cole L.A., and Perdew J. (1982). Calculated Electron Affinities of the Elements. Phy. Rev. A 25:1265.

[35] Becke A.D. (1988). Density-Functional Exchange-Energy Approximation with Correct Asymptotic Behavior. Phy.Rev. A **38**, 3098.

[36] Lee C., Yang W., and Parr R.G. (1988). Development of the Colle-Salvetti Correlation-Energy Formula into a Functional of the Electron Density. Phy. Rev. B **37**, 785.

[37] Perdew J.P., Burke K., and Ernzerhof M. (1996).

Generalized Gradient Approximation Made Simple. Phy. Rev. lett. **77**, 3865.

[38] Chiodo L., García-Lastra J.M., Iacomino A., Ossicini S., Zhao J., Petek H.. (2010). Self-Energy and Excitonic Effects in the Electronic and Optical Properties of Tio 2 Crystalline Phases. Phy. Rev.B **82**, 045207.

[39] Labat F., Baranek P., Domain C., Minot C., and Adamo C. (2007). Density Functional Theory Analysis of the Structural and Electronic Properties of TiO_2 Rutile and Anatase Polytypes: Performances of Different Exchange-Correlation Functionals. The J. of Chem. Phy. **126**, 154703.

[40] Yang K., Dai Y., Huang B. (2007). Understanding Photocatalytic Activity of S-and P-Doped TiO_2 under Visible Light from First-Principles. The J. of Phy. Chem. C **111**,:18985-94.

[41] Li N., Yao K., Li L., Sun Z., Gao G., and Zhu L. (2011). Effect of Carbon/Hydrogen Species Incorporation on Electronic Structure of Anatase-TiO_2. J. of App.Phy. **110**, 073513.

[42] McLeod J., Green R., Kurmaev E., Kumada N., Belik A., and Moewes A. (2012). Band-Gap Engineering in Tio 2-Based Ternary Oxides. Phy. Rev. B **85**, 195201.

[43] Zhang Y.G., Wang Y.X. (2011). Calculations Show Improved Photoelectrochemical Performance for N, Ce, and Ce+ N Doped Anatase TiO_2. .J. of Applied Physics **110**, 033519.

[44] Khan M., Xu J., Chen N., and Cao W. (2012). Electronic and Optical Properties of Pure and Mo Doped Anatase Tio2 Using Gga and Gga+ U Calculations. Physica B: Cond Matter **407**, 3610-6.

[45] Khan M., Xu J., Chen N., Cao W., Usman Z., and Khan D. (2013). Effect of Ag Doping Concentration on the Electronic and Optical Properties of Anatase Tio 2: A Dft-Based Theoretical Study. Research on Chem Intermediates **39**, 1633-44.

[46] Zhang R., Wang Q., Li Q., Dai J., and Huang D. (2011). First-Principle Calculations on Optical Properties of C–N-Doped and C–N-Codoped Anatase TiO_2. Physica B: Cond. Matt. **406**, 3417-22.

[47] Zhang R., Wang Q., Liang J., Li Q., Dai J., Li W. (2012). Optical Properties of N and Transition Metal R (R= V, Cr, Mn, Fe, Co, Ni, Cu, and Zn) Codoped Anatase TiO_2. Physica B: Cond. Matt. **407**, 2709-15.

[48] Liu X., Jiang E., Li Z., and Song Q. (2008). Electronic Structure and Optical Properties of Nb-Doped Anatase TiO_2. App Phy. Lett. **92**, 252104.

[49] Guo M., and Du J. (2013). Electronic and Optical Properties of C–N-Codoped TiO_2, A First-Principles Gga+ U Investigation. Inter J. of Modern Phy. B **27**, 1350123.

[50] Lei Y., Liu H., and Xiao W. (2010). First Principles Study of the Size Effect of TiO_2 Anatase Nanoparticles in Dye-Sensitized Solar Cell. Modelling and Simulation in Materials Science and Engineering **18**, 025004.

[51] Linsebigler A.L., Lu G., and Yates Jr J.T. (1995). Photocatalysis on TiO_2 Surfaces: Principles, Mechanisms, and Selected Results. Chem. Rev 95:735-58.